5-2020

Estimating the Displacement on the Norumbega Fault System Using Quartz Microstructures

Christopher T. Sargent

Estimating the Displacement on the Norumbega Fault System Using Quartz Microstructures

A Senior Thesis

Presented to the Faculty of the Department of Geology Bates College in partial fulfillment of the requirements for the Degree of Bachelor of Arts

By

Christopher T. Sargent

Lewiston, Maine
December 15, 20

Acknowledgements

A special thanks to everyone who made this project and research possible. To the Bates Student Research Fund for allowing me to conduct research using the Scanning Electron Microscope, to Professor Calvin Mako for his support and his wise thoughts, to Emily Peterman for making my SEM research possible, to the Bates College Geology Department for assisting with research, Dykstra Eusden for encouraging me to peruse geology and to all my classmates who encourage and pushed me during this process.

Table of Contents

List of Figures

List of Tables and Equations

Abstract

The Sandhill Corner shear zone is the longest continuous strand of deformation within the Norumbega Fault System (NFS). The Norumbega is a dextral fault system that extends from New Hampshire into New Brunswick. This study uses recrystallized grain size piezometry and quartz flow laws to determine the total offset on the Sandhill Corner shear zone (SCsz). Recrystallized quartz grains were measured and quartz crystallographic preferred orientations (CPO) were determined in three samples using SEM-EBSD. Differential stress and deformation temperature can be estimated from these data and then used to calculate strain rate and total shear zone offset. Calculating the quartz c-axis fabrics made it possible to determine the deformation temperature, these temperatures ranged from 400±50ºc to 500±50ºc. Differential stress ranged between 47.5-60.1MPa, the strain rate ranged between $1.44 x 10^{-13} s^{-1}$ and $3.73 x 10^{-13} s^{-1}$ and the plate velocity estimates were between 0.45-1.18cm/year.

Previous estimates of the total displacement across the Norumbega fault system and the Sandhill Corner shear zone range widely, from 25-1900km. Based on a previously well-established regional cooling history there was significant plate movement during a 30-million-year period. Based on deformation temperature and published Ar-Ar dating, it was possible to estimate that this shear zone was deforming between 370 million years ago to 340 million years ago. It was possible to get an estimated total distance of displacement between 136-353km.

Introduction

Purpose of Study

The Norumbega fault was an active shear zone from the Devonian to Carboniferous time (370-290Ma). It is a dextral shear zone that stretches from southern Maine to New Brunswick (Bothner and Hussey, 1999). This fault system is one of the longest and most studied fault systems in the northeastern US. The fault system cuts through the Appalachian Mountains and is part of the complex record of orogenesis and metamorphism in New England. Determining the deformation conditions is essential for learning about the development of major shear zones like the Norumbega. Some of these important conditions include the temperature of deformation, strain rate, differential stress, plate velocity and the duration of shear zone movement within the fault. These deformation conditions are the parameters when determining the overall displacements of the fault. This study focuses on the recrystallization size of quartz grains within the Sandhill Corner shear zone to determine strain, differential stress and total displacement of the fault.

Active shear zones accommodate the large-scale movement of tectonic plates, which causes the minerals within shear zones to be deformed and recrystallized. The recrystallized grains are often the key to determining the history of that shear zone. Multiple episodes of deformation make interpreting shear zone microstructures especially challenging; these microstructures are overprinted with a new record of the conditions of deformation. The quartz microstructures are particularly useful for understanding shear zone deformation. By examining these microstructures, crystallographic preferred orientations (CPO), grain size and the grain boundary morphology it is possible to constrain the deformation temperature and ultimately the total displacement. Determining the magnitude of differential stress and strain rate from these data are essential steps to understanding the larger picture of the total fault offset.

The primary purpose of this study is to examine the quartz microstructure within a section of the Norumbega fault system known as the Sandhill Corner shear zone (Figure 1) (Price at al., 2016; Bothner and Hussey, 1999). A series of mylonite samples from this shear zone were collected, made into thin sections. They were then examined using a Scanning Electron Microscope (SEM) and Electron Backscatter Diffraction (EBSD) to determine the size and crystallographic preferred orientations (CPO) of the recrystallized quartz grains. The CPOs and the grain sizes are necessary when determining the deformation temperature and the differential stress. These values can then be used calculate the strain rate which will make it possible to find the plate velocity and finally the total displacement.

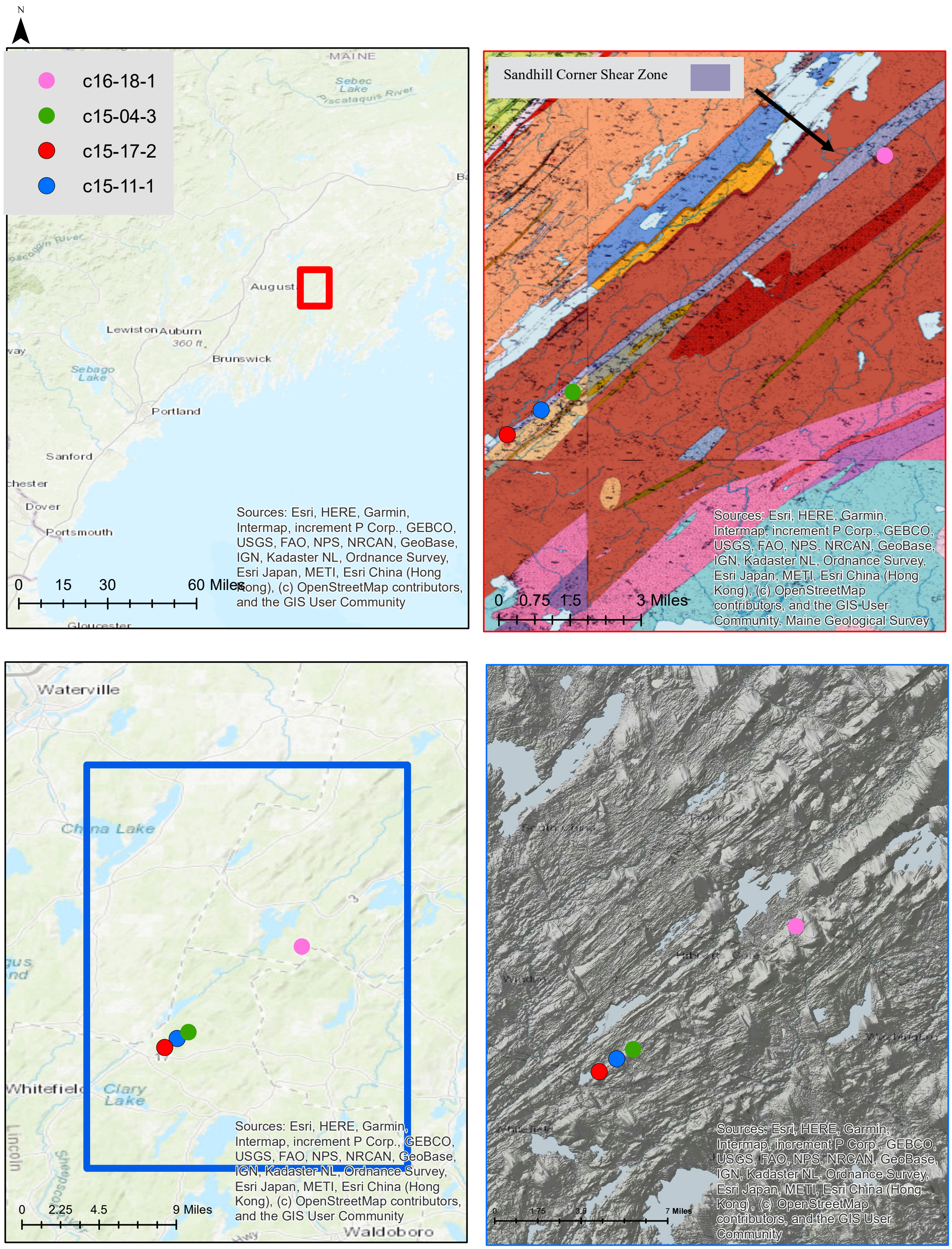

Figure 1. The samples were all collected from an area in or near the Sandhill Corner shear zone. The Norumbega Fault system and the Sandhill Corner shear zone go directly along the coast of Maine. See Figure 2 for more detailed geology of this area. Sample coordinates are available in Appendix D.

The Norumbega Fault Zone

The northeast Appalachians represent the culmination of a complex mess of orogenesis, metamorphism and plutonism. The dextral deformation associated with the Norumbega fault system adds to its complexity (West,1999). The southern portion of the Norumbega fault system contains a 5-40 km wide zone that is characterized by heterogeneous non-coaxial, dextral deformation that occurred in peak metamorphic conditions (Price et. al., 2016). The deformation within this shear zone likely began around 370 million years ago and possibly came to an end around 290 million years ago (West and Lux, 1993; Ludman et al., 1999). There have been many estimates of overall displacement in the NFS, the range is 30-1900km of total displacement (West and Lux, 1993; Ludman et al. 1999; Hubbard, 1999).

The specific area within the Norumbega Fault system that this paper will focus on is the Sandhill Corner shear zone (Figure 2). This shear zone is the longest continuous strand of the deformation part of the Norumbega Fault System (Price et al., 2016). The Sandhill Corner shear zone is an example of a high-strain zones and is around 300-500m wide. The shear zone is composed of mylonites and ultralmylonites derived from quartz and feldspar-rich rocks. The two distinct formations that are cut by the Sandhill Corner shear zone are the Cape Elizabeth Formation and the Crummett Mountain Formation (Bothner and Hussey, 1999; Price at al., 2016). The Cape Elizabeth formation is a metasedimentary unit that was partially magmatized and metamorphosed (Price at al., 2016). It is estimated from U/Pb ages that the Cape Elizabeth formation is older than 469 ± 6Ma (Bothner and Hussey, 1999). The Crummett Mountain Formation is a graphite-rich, pelitic schist with folds and boundinaged layers of calc-silicate granofels (Price at al., 2016). The Sandhill Corner shear zone has an NE-striking subvertical foliation with an average orientation of 37º/88º NW and a subhorizontal mineral lineation averaging of 5º/37º. The deformation within the Sandhill Corner shear zone is superimposed on an earlier high-temperature shear fabric (Price at al., 2016). Previous work has found that the microstructures within the Sandhill Corner shear zone suggested that deformation was dominated by dislocation creep and that the microstructures are consistent with a temperature of mylonitization of 300-500ºC (West and Lux, 1993; Stipp et al., 2002; Passchier and Trouw, 2005; Price et al. 2012; Price at al., 2016). One of the aims of this study is to make a more precise estimate of the deformation temperature.

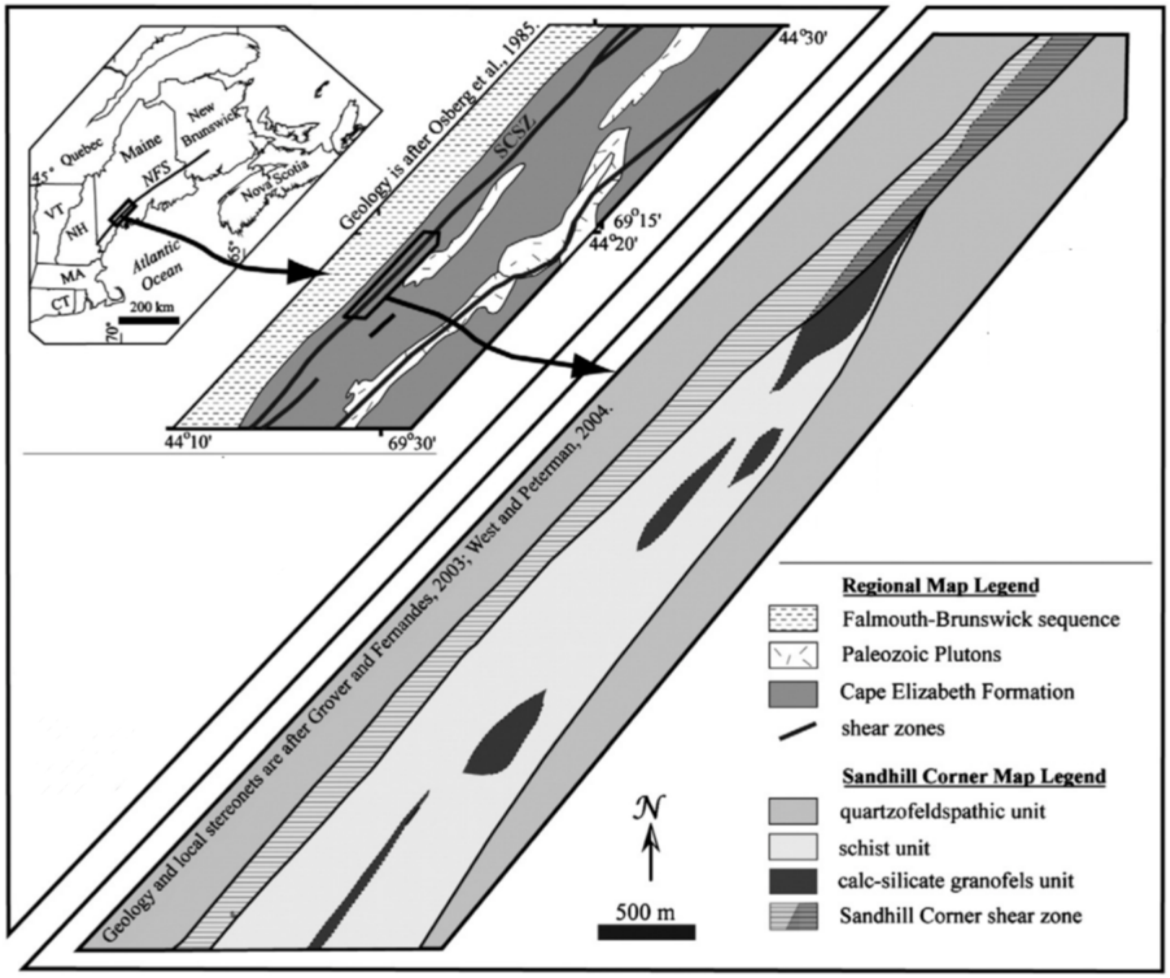

Figure 2. Norumbega Fault System illustrated in the top left of the map with NFS. The Sandhill Corner shear zone is illustrated in the top left with the small box and then the larger geological map as SCSZ. Notice the various tock types that the Sandhill Corner shear zone is bordering. This shear zone is a high-strain zones; the shear zone is around 300-500m wide and is a northeast striking subvertical, mylonitic shear zone that is the contact in-between two formations; the Cape Elizabeth Formation and the Crummett Mountain Formation (Crummett not labeled here but the rock type is here) Price et al. 2016.

Quartz Deformation Microstructures

Microstructures are the key to determining the kinematics, deformation conditions and evolution of a shear zone. Within the Sandhill Corner shear zone monomineralic quartz veins are plentiful and fantastic indicators of the deformational history. Specifically, this study uses quartz microstructures to determine the deformational temperature, differential stress, strain rate and total deformation.

A first order constrain on the deformation temperature in a shear zone can be made using quartz recrystallization textures, which can be examined using optical microscopy. The recrystallization mechanisms will help to get an idea of what metamorphic temperatures were acting on the Sandhill Corner shear zone. There are three types of recrystallization mechanisms and each are associated with a range of metamorphic temperature. Bulging (BLG) is low-temperature recrystallization mechanisms, this occurs between 300-400ºC (Stipp et al., 2002). Bulging occurs when two touching grains have different dislocation density the grain boundaries migrate or 'bulge' into one another. The grain with the lower dislocation density will intrude into the higher density grain (Figure 3) (Passchier and Trouw, 2005; Price at al., 2016). Subgrain Rotation occurs at medium-high metamorphic temperature, this occurs in the range of 400-500ºC (Passchier and Trouw, 2005; Price at al., 2016). Subgrain Rotation (SGR) occurs when dislocations accumulate and cause small areas of a crystal to have a different crystallographic orientation than the rest of the crystal (Figure 3) (Stipp et al., 2002). Grain boundary migration (GBM) occurs at high temperature metamorphism, this temperature range is between 500-700ºC (Passchier and Trouw, 2005; Price at al., 2016). GMB occurs when the high temperature makes it possible for the grain boundaries to be more mobile, this allows the grain boundaries to move around similarly to SGR. In GBM the new grains are often larger than in SGR and rather than a uniform border movement it is sporadic (Figure 3) (Stipp et al., 2002). In BLG, the bulges are on a much smaller scale than the 'wavy' appearance of the GBM grain boundaries. Determining if the quartz grains are undergoing BLG, SGR or GBM recrystallization will give the broad temperature conditions of deformation.

A more precise estimate of deformation temperature can be obtained using the quartz c-axis fabric opening angle (Law, 2014). During recrystallization, quartz CPOs can develop a cross girdle pattern. Research has found that this cross girdle is related to deformation temperature. This makes it possible to measure the angle between the girdle and from this make an estimate of temperature.

The grain size of recrystallized quartz has been experimentally calibrated to differential stress during deformation (Stipp and Tullis, 2003; Holyoke and Kronenberg, 2010). The numerical relationship between grain diameter and the differential stress is shown in Equation 1 (Holyoke and Kronenberg, 2010). The differential stress and the deformation temperature can be used to determine the strain rate based on a quartz flow law, which is an equation that is experientially derived (Equation 2) (Hirth et al., 2001). The flow law calculates the fault strain rate or how fast the deformation is. The strain rate can be used to determine the plate velocity using Equation 3, which also incorporates the total width of the shear zone during deformation (Platt, 2015).

Finally, these estimates of strain rate and plate velocity can only be used if the total duration of deformation is known. The well-established regional cooling history is used to find the approximate end of deformation (West and Hussey, 2016). Once the end of deformation was found it made make it possible to find the entire duration of deformation. The place velocity can be multiplied by the duration of plate movement to determine the total displacement recorded by the Sandhill Corner shear zone.

$$D = 2451\sigma^{-1.26}$$

Equation 1. Differential stress Equation, where D represents grain diameter (µm), and σ is differential stress (MPa) (Holyoke and Kronenberg, 2010).

$$\varepsilon = Af_{H_20}^{m}\sigma^{n} \exp\left(-\frac{Q}{RT}\right)$$

Equation 2. Flow Law Equation. The material parameter (A) has a value of 10-11.2±0.6 MPa, water fugacity exponent (m) has a given value of 1, the stress exponent (n) has a given value of 4, the activation energy (Q) has a given value of 135±15KJ/mol and the ideal gas constant (R) has a value of 8.314. The water fugacity (F), differential stress (σ), temperature (T) and strain rate (ε) are not givens and are determined in throughout this study. (Hirth et al., 2001).

$$\mathrm{W} = \frac{V}{2\varepsilon}$$

Equation 3. Plate Velocity Equation. To calculate plate velocity (V) you must first find the strain rate (ε) and width (W) (Platt, 2015).

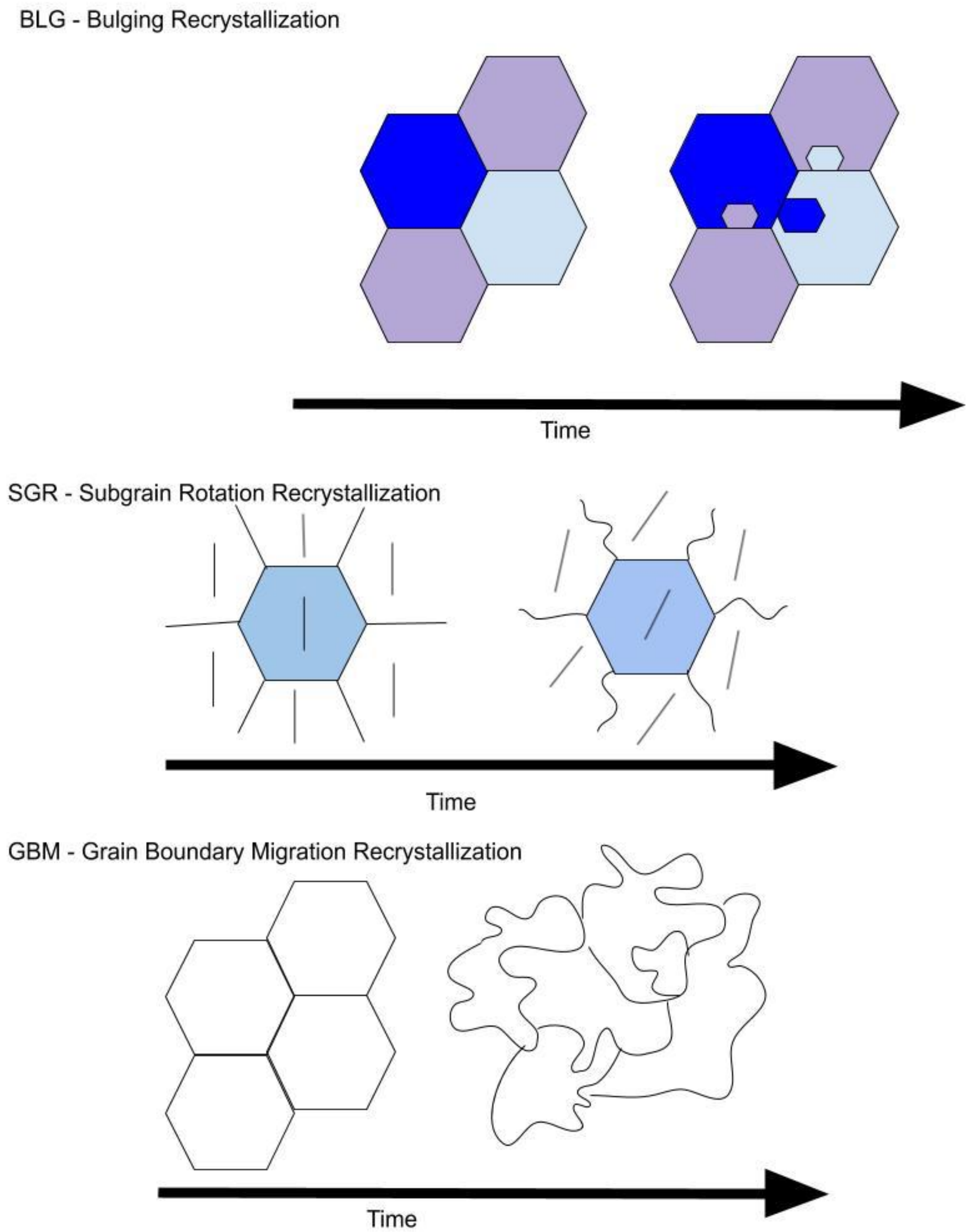

Figure 3. The three main types of recrystallization, Grain Boundary Migration (GBM), Subgrain Rotation (SGR), Bulging (BLG). Bulging (BLG) shows two touching grains have different density, the grain with the lower density intrudes into the higher density grain. Subgrain Rotation (SGR) occurs when the angles on both sides of the subgrain boundary continue to increase until the subgrain can no longer be classified as the same grain and a new grain will be created in the process. The middle line within each of the grains represents the quartz c-axis, during SGR this also rotates. GBM is a high temperature recrystallization, new grain boundaries movements sporadic and is able to have a much larger range of movement. Modified by Chris Sargent and based on Passchier and Trouw, 2005, p. 42.

Methods

Overview

Samples were collected from the Sandhill Corner shear zone between 2015 and 2016 (Figure 1). The samples were selected from the host rocks or within the shear zone. Four of the samples were selected to use for this study, these samples were selected based on the abundance of quartz veins and strong kinematic indicators. Data was collected and analyzed to determine the grain size and the quartz c-axis fabric opening angle of the quartz microstructures. The grain orientation and opening angles helped to determine temperature and the grain size helped to determine differential stress. Once temperature and differential stress were obtained it was possible to use the flow law equation (Hirth et al., 2001) to determine the strain rate. Both the strain rate and the differential stress values made it possible to determine the plate velocity and deformation duration. By knowing these parameters, it is possible to calculate the total offset.

Lab Methods

Scanning Electron Microscopy and Electron Backscatter Diffraction

Samples C15-11-1, C15-17-2, and C16-18-1 were selected for analysis. The three samples were examined under a petrographic microscope and selected for SEM because they contain areas of nearly pure quartz. This is essential for quartz grain size piezometry because the quartz grains are not pinned by other phases that would stop recrystallization. The samples were then taken to Bowdoin College to examine the quartz grains using SEM and EBSD. To prep for the SEM a carbon coat was put on each of the thin sections. Using a Cressington 108 Carbon/A with a film thickness monitor, between 5-8nm of carbon was placed on each thin section (Figure 4). A carbon coat is useful for EBSD when dealing with minerals because it prevents ion charging within the chamber. Once the samples were covered with carbon, they were ready to place in the SEM chamber.

SEM uses a high-energy electron beam to image and analyze samples at an extremely high resolution. EBSD is an attachment for the SEM (Figure 5) that is used to determine the crystallographic orientation of a mineral (Schwartz et al., 2000). EBSD uses backscattered electrons that are emitted when the high-energy electron beam hit the minerals (Swapp, 2019). EBSD patterns are made on a phosphor screen by the electron's diffraction of the high-energy electron beam (Schwartz et al., 2000). The geometry of the mineral pattern can be a representation as a two-dimensional projection of the mineral's three-dimensional crystal lattice (Schwartz et al., 2000). The EBSD collects orientation data in a raster grid across the sample and will only collect the mineral pattern of the minerals if it matches the quartz mineral pattern (Figure 6). Later, the individual grains are defined in the post-processing phase. Using the EBSD will help to provide the quartz crystallographic preferred orientation (CPO) which will help to determine the deformation temperate. Quartz grains are determined by merging adjacent raster pixels with similar orientation. From this grain sizes can be calculated, which will help to determine the differential stress (Schwartz et al., 2000, Fossen, 2016).

The SEM at Bowdoin College is a Tescan Vega3 LMU model, and it equipped with an HKL Nordlys II detector (Figure 5). Multiple tests were done on each of the samples to optimize the operating conditions. The EBSD collected data at step sizes of 5μm and 10μm. The CPO data was relatively similar between the two step sizes, however, 5μm step size showed a higher resolution grain size. Due to limited time it was only possible to complete analysis on three of the four originally samples selected. Conditions were similar for each sample so it would be possible to compare the results from each sample.

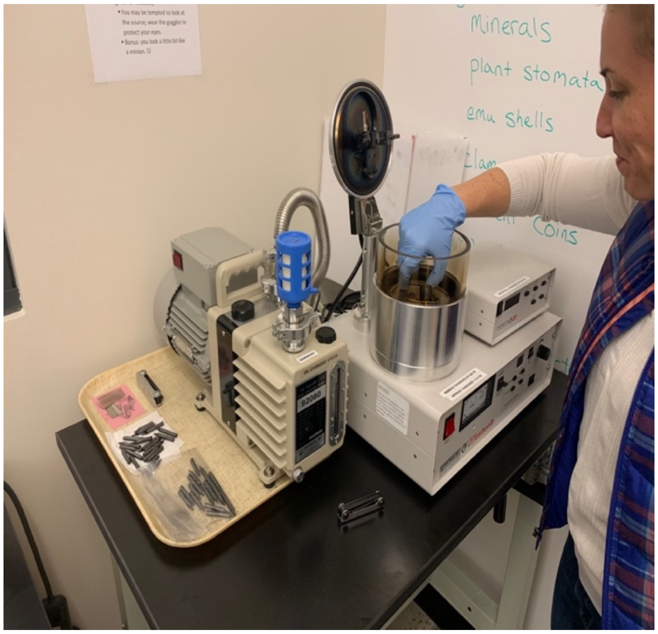

Figure 4. Cressington 108 Carbon/A with a film thickness monitor. Here Emily Peterman, Bowdoin College, is placing C16-18-1 in the Cressington to get carbon coated. We applied between 5-8nm of carbon to each thin section to eliminate the amount of ion charging

Figure 5. Bowdoin College's SEM, a Tescan Vega3 LMU model, and equipped with an HKL Nordlys II detector. This was the main tool for our analysis.

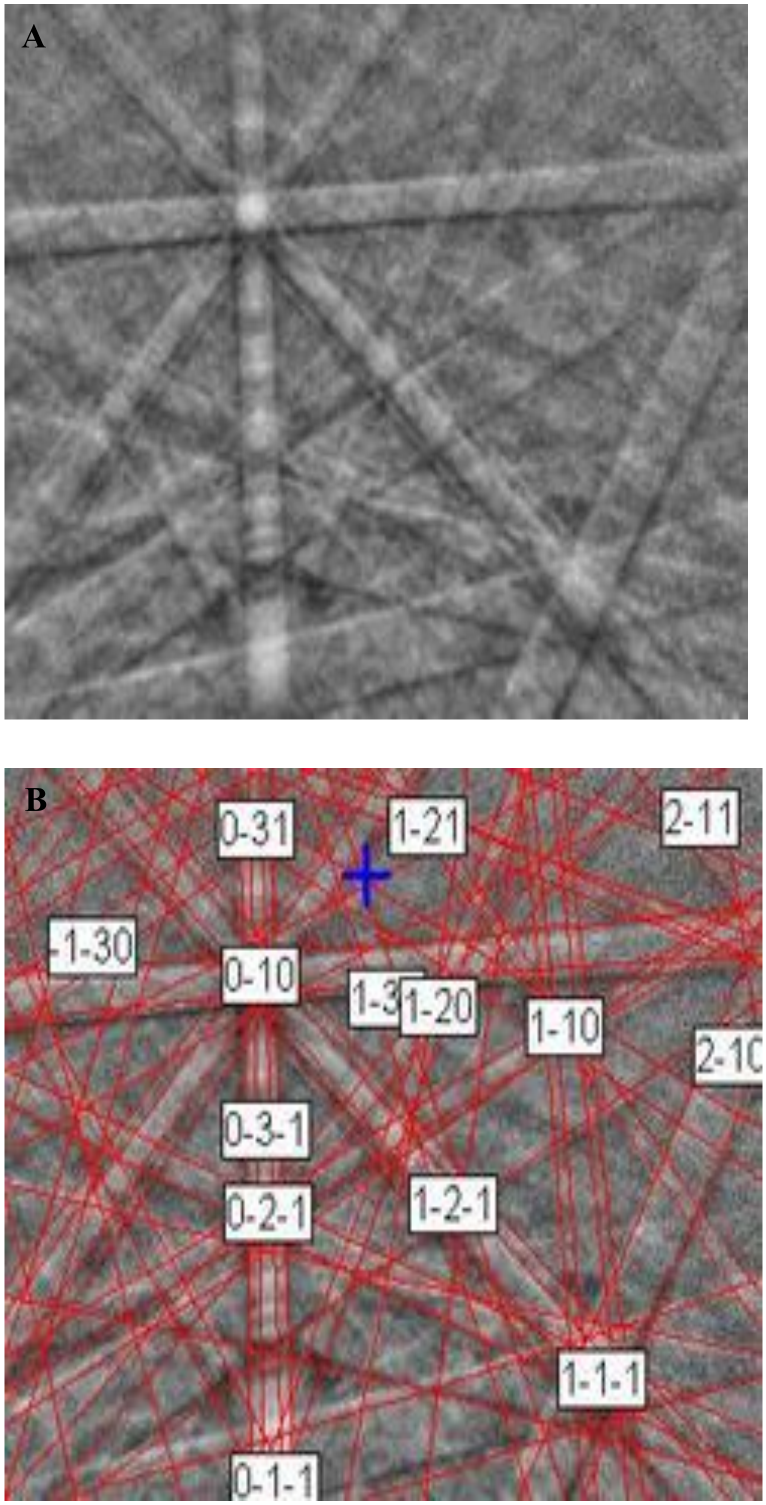

Figure 6. A. Quartz diffraction bands or the mineral pattern. B. The software identifying that the mineral lattice plane of the mineral being analyzed corresponds with the diffraction bands in A. It will only collect data if it recognizes that it is a quartz grain. (Schwartz et al., 2000, Swapp, 2019).

Sample Conditions

The conditions for the EBSD and the SEM were kept as constant as possible for future reproduction and to make it easier to make comparisons between samples. The chamber pressure was 10-15Pa, beam intensity was at 20 kV, the working distance was 26.4mm, the samples had a 70º tilt towards the EBSD and the EBSD detector had a position of 130mm. First, small areas of the quartz veins were examined by doing a trial run. These tests were done to get a basic idea of the grain size and determine if a step size 5µm or 10µm was appropriate. Then larger areas of the quartz veins were analyzed, in most cased it was not possible to scan the entire quartz veins because of time limitations. The scans took as little as 0.75 hours and as long as 20 hours.

Post Processing

First, the data was collected in Aztec, version 3.12, this software is directly transferred from the EBSD and makes it possible to view live EBSD scans. After the scans were concluded the data was converted and placed in Channel 5 to clean up the data (Bachman et, al., 2010). First, the randomly oriented pixels were removed to ensure that they did not influence the grain diameter data. This process selects individual grains that were dissimilar to the ones around it and remove that point to keep outliers out of the data set. Next, the non-indexed pixels were extrapolated by 8, 7 then 6 closest neighbors. Extrapolation is when the software selects the non-indexed pixels and uses the average orientation of its 8 neighbors to create an orientation for the non-indexed pixel. This process is then done again with 7 neighbors then 6 neighbors. Extrapolation is done to ensure that the data is a representation of the whole quartz grains rather than just single pixels. Channel 5 then determined the quartz grain diameter of the remaining grains. To do this the software had to select which pixels made up a quartz grain. A mis-orientation angle of 10º was used to select between different grains.

MATLAB was used to run MTEX, which is a coding toolbox specifically designed for EBSD analysis. This was used to convert the c-axis orientations into a stereonet which made it possible to obtain a quartz c-axis fabric opening angle (Schmidt and Olesen, 1989). The quartz c-axis orientations were plotted on a contoured stereonet. The contoured stereonets made it possible to measure a quartz c-axis fabric opening angle which would determine the deformation temperature (Law, 2014; Fossen, 2016).

Determining Fault Displacement

The fault displacement is based off finding the speed the plates were moving and for how long deformation was occurring. To find the plate velocity it is first necessary to know the strain rate. The strain rate, which is calculated from the flow law, requires values for differential stress and deformation temperature. The differential stress can be calculated by finding the quartz grain diameter and then using Equation 1 (Holyoke and Kronenberg, 2010) (Figure 7). The temperature is calculated from measuring the quartz c-axis fabric opening angle and finding the associated deformation temperature (Figure 8). Once these variables are found it is possible to use the flow law to calculate the strain rate (Equation 2) (Hirth et al., 2001). The duration of the fault can be estimated by assigning the start of deformation to 370Ma (Ludman et al., 1999) and using geochronology and deformation temperature to determine when deformation ended (West and Hussey, 2016). Plate velocity can be calculated by using Equation 3 which multiples strain rate by the width of the shear zone (Platt, 2015). Once the plate velocity and the duration are determined it is possible to determine the displacement. The final calculation to discover displacement is found by simply multiplying velocity of the plates by the duration of deformation.

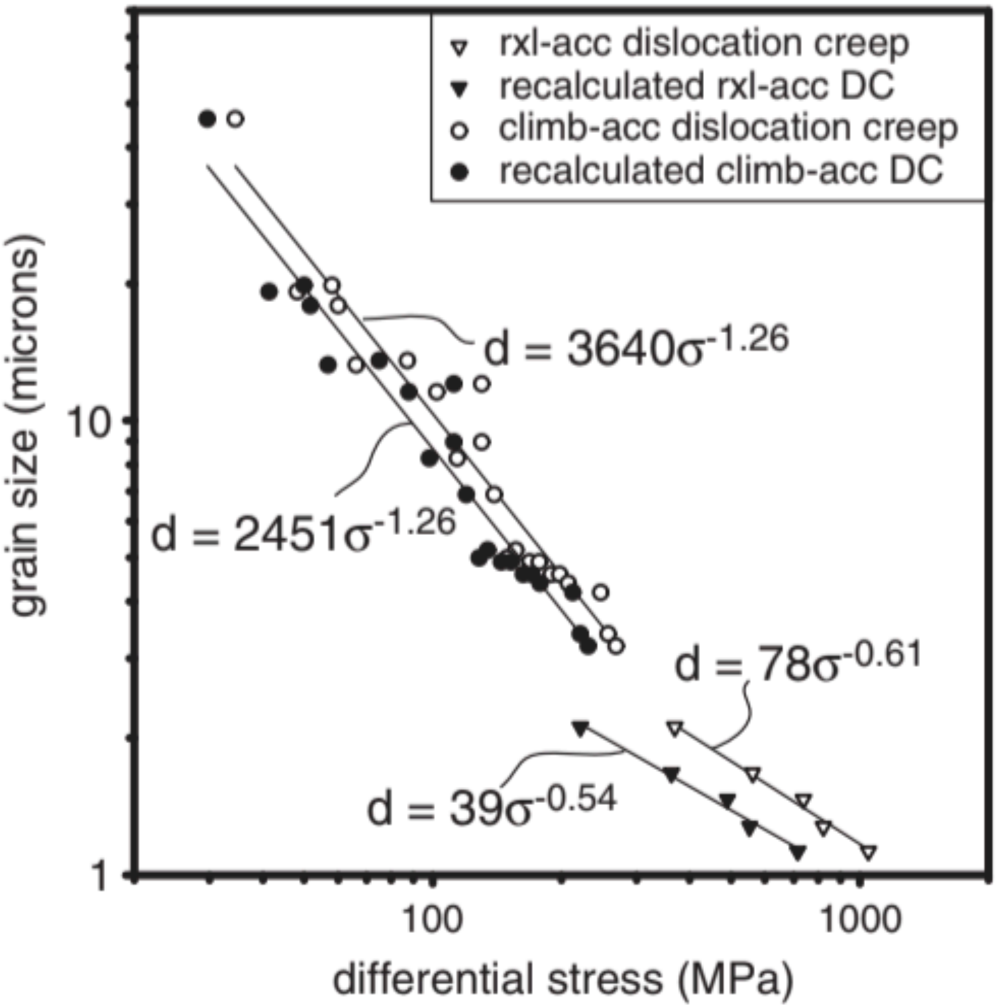

Figure 7. Grain size and differential stress graphic. This is the experimental data that the grainsize-stress calibration corrected using the MSC calibration (solid circles) (Holyoke and Kronenberg, 2010). This equation was calculated by Stipp and Tullis, 2003 and later corrected by Holyoke and Kronenberg, 2010.

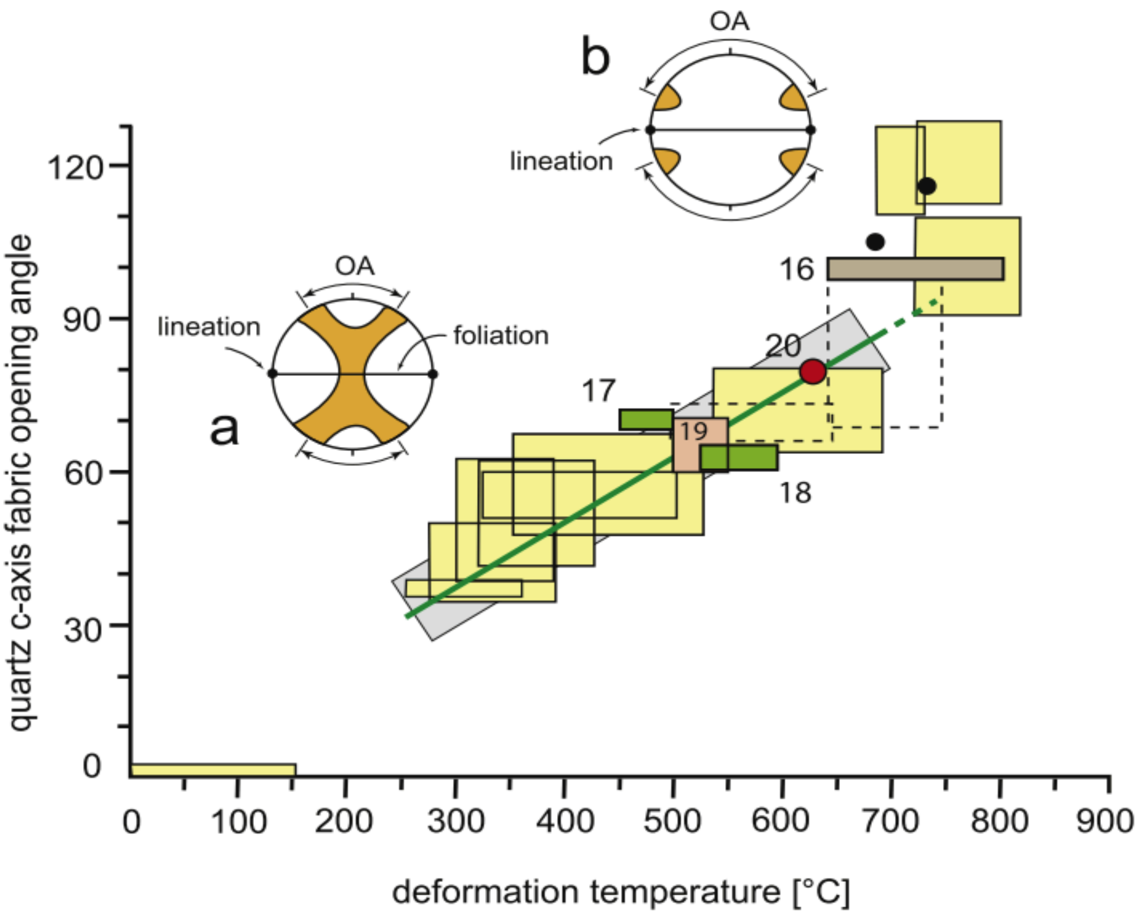

Figure 8. The relationship between quartz c-axis fabric opening angle and deformation temperature (Law 2014).

Results

Microstructures

Optical Microscopy

Kinematic indicators and deformation mechanisms were examined using a petrographic microscope. In sample C15-04-3, small quartz grains can be seen intruding into other quartz grains in a way that is also seen in BLG deformation (Figure 9). While looking through the petrographic microscope there were many delta clasts and porphyroclasts which are indicators of non-coaxial deformation (Figure 10). Additionally, feldspars in this sample show brittle deformation structures, indicating that deformation temperature was below 500ºC (Figure 11) (Passchier and Trouw, 2005). In sample C15-11-1 there are clear mica fish, which are also indicators of non-coaxial deformation (Figure 12) (Passchier and Trouw, 2005). Samples C16-18-1, C15-11-1 and C15-17-2 show rotations of the quartz grain boundaries, this is an indicator of SGR (Figure 10). Based on the quartz deformation mechanisms and the brittle feldspar defamation, the deformation temperature was likely above 280ºC and less than 500ºC.

Electron Backscatter Diffraction

It is possible to compare the quartz grains in the optical and the EBSD images. The individual quartz grains were easier to distinguish with EBSD images, rather than optically. (Figure 13-16). In sample C15-11-1, it is hard to identify some of the quartz grains, by using the EBSD it made this easier (Figure 14). In sample C15-17-2, the two quartz veins that were focused on become much clearer and quartz grains are very visible when using the EBSD photos (Figure 15 and Figure 16). While using the EBSD, samples were analyzed at both 5µm and 10µm**.** When comparing the scans that were done at these step sizes it is clear that the 5µm produces a much higher resolution scan of the grains, this will be discussed more in later sections (Figure 15 and Figure 16). The ability to view these samples both under a petrographic microscope and the EBSD, helps to bring clarity and confidence when examining the quartz grains.

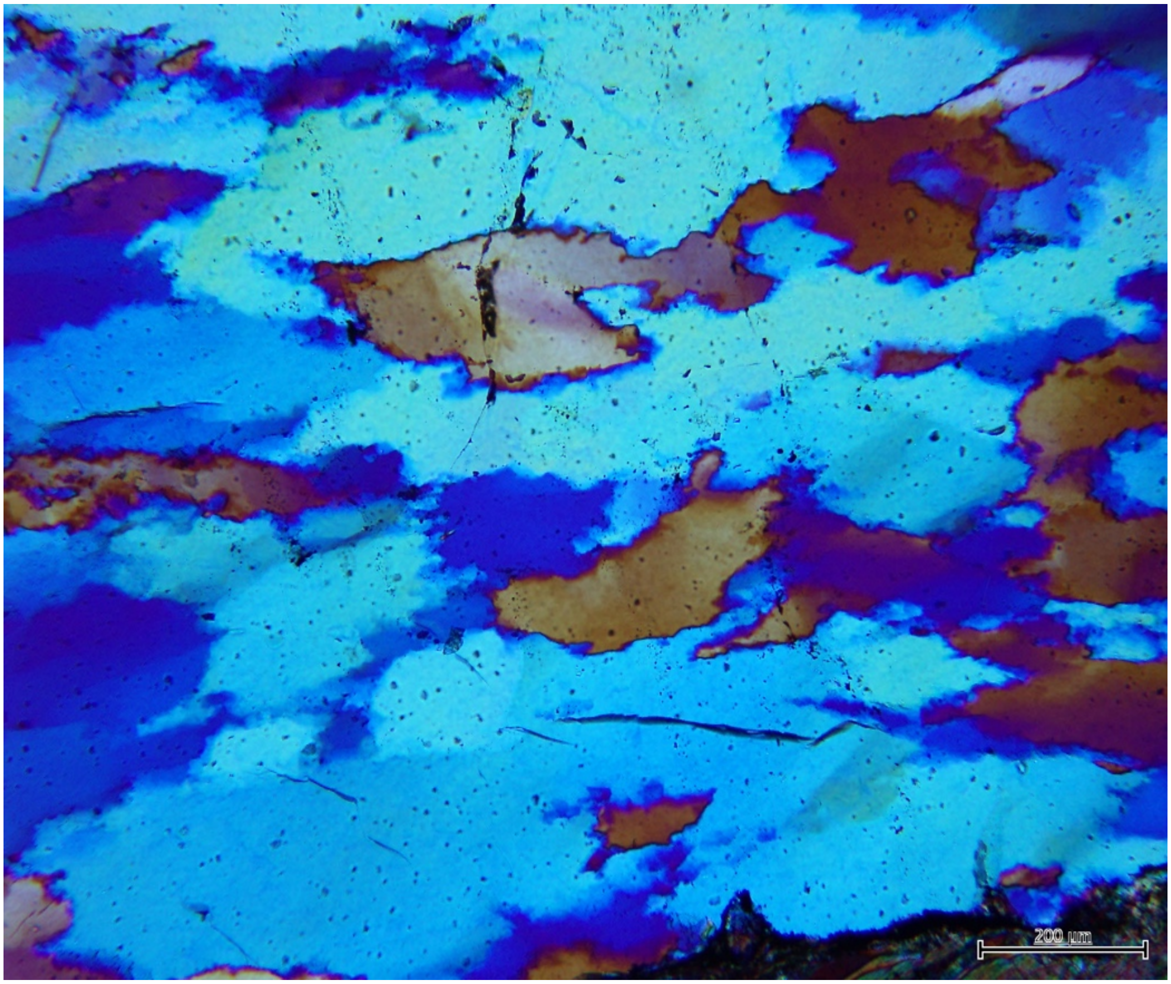

Figure 9. Sample C15-04-3 showing a good example of BLG which is an indicator that the deformation was around 400ºC. This image was taken using a gypsum plate.

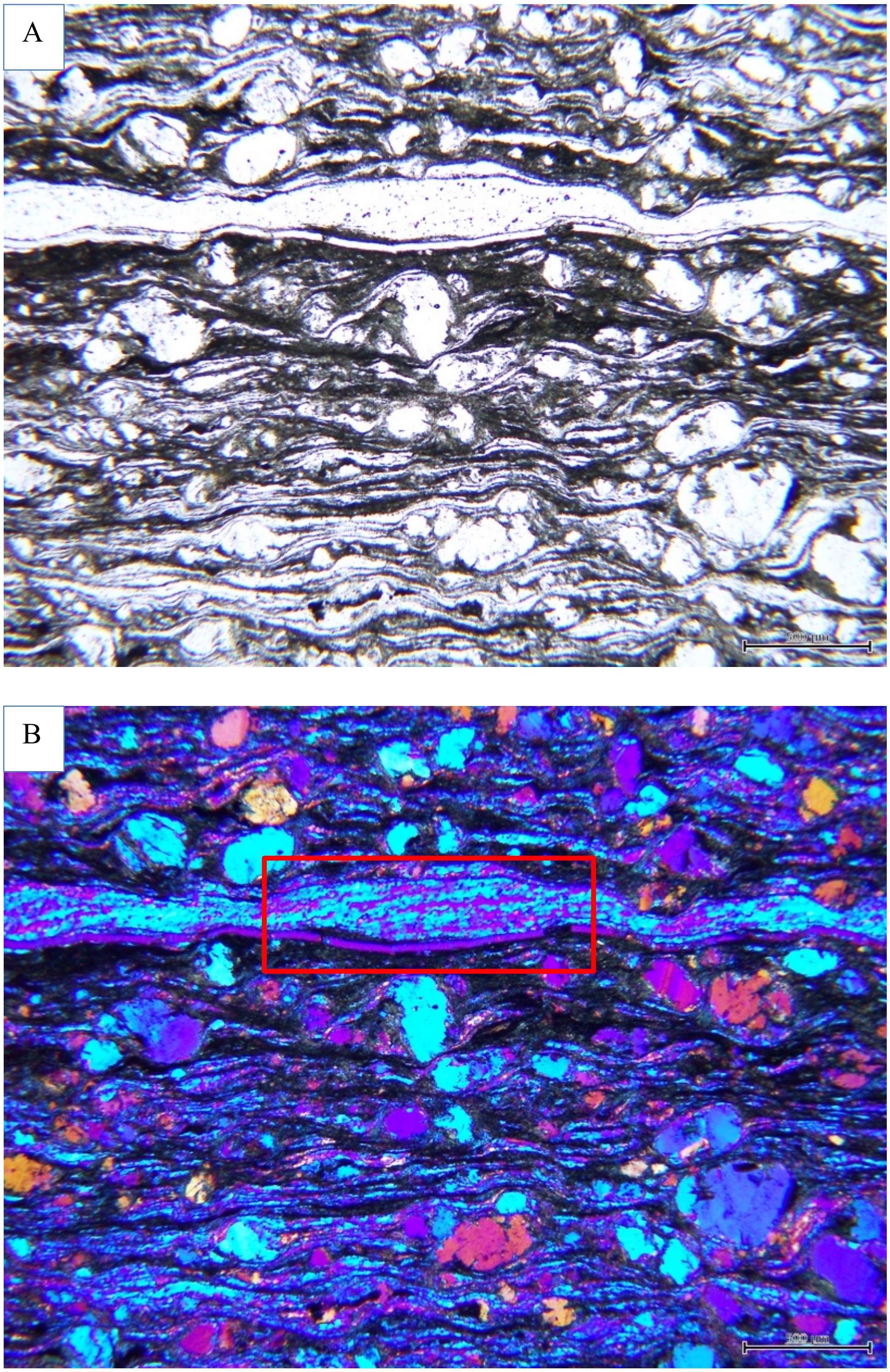

Figure 10. Sample C16-18-1. The delta clast that is an indicator of non-coaxial deformation. Examined under, A, cross polarized light and, B, using a gypsum plate. The red box shows an area that shows SGR.

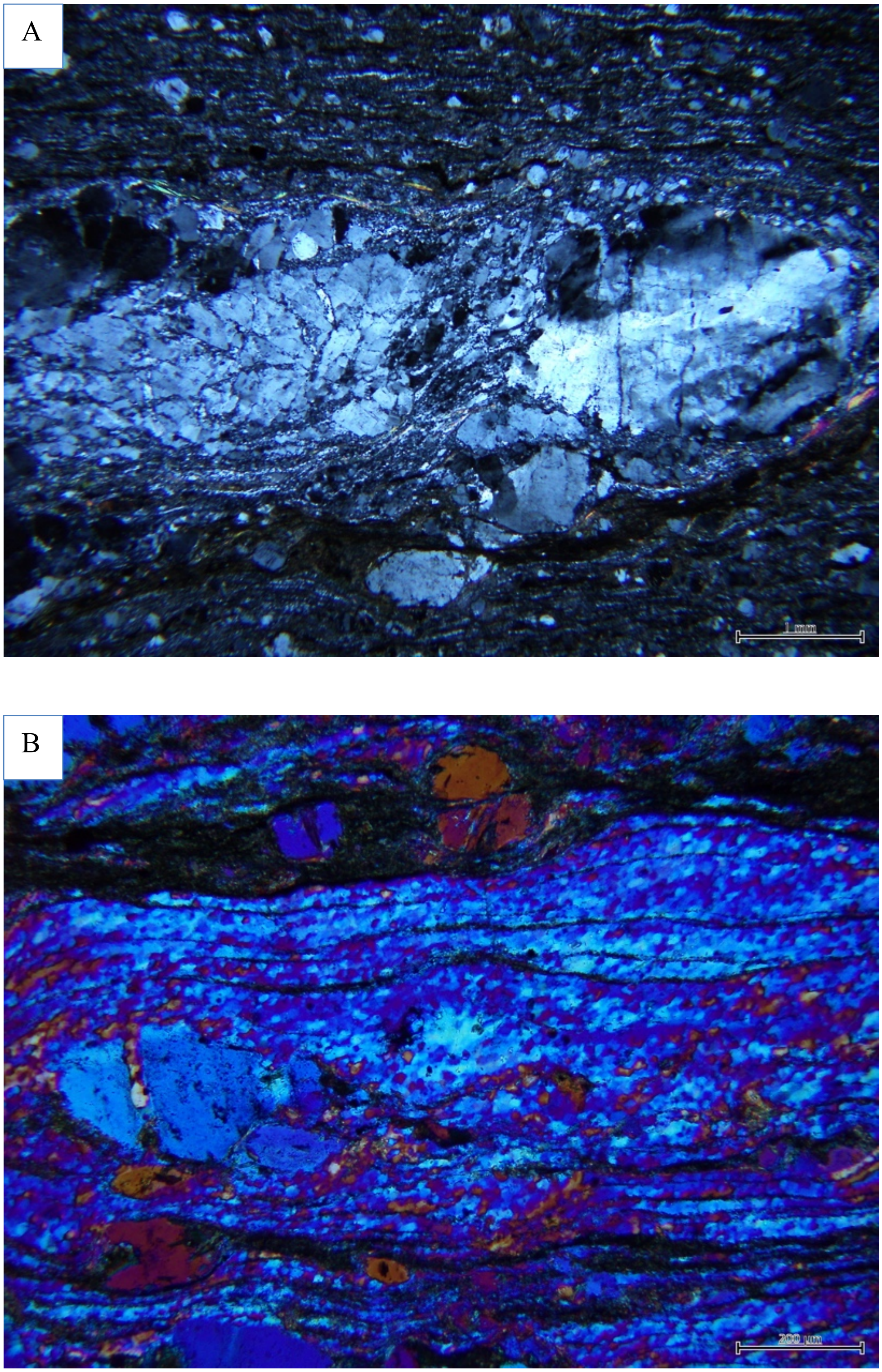

Figure 11. Sample C16-18-1. Brittle feldspar deformation which indicate a deformation temperature below 500ºC. Examined under, A, cross polarized light and, B, using the gypsum plate.

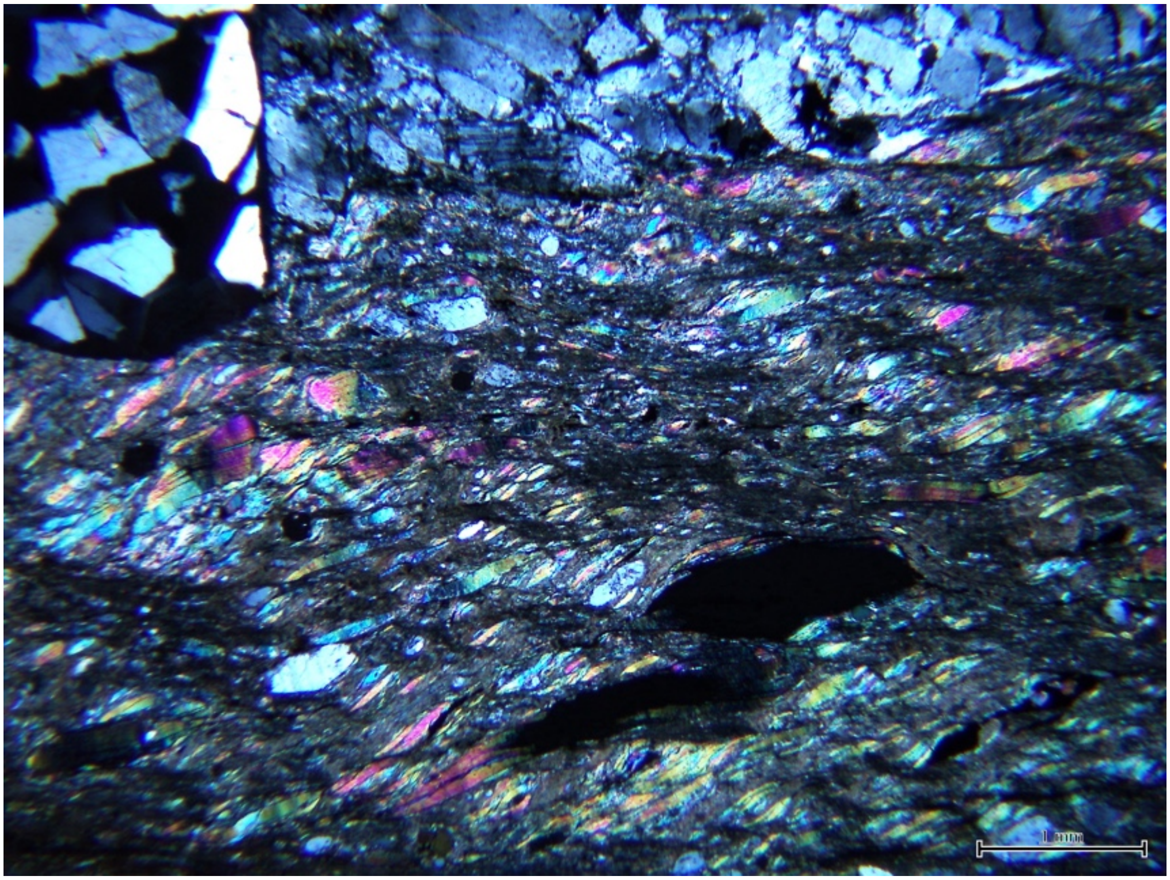

Figure 12. Sample C15-11-1. Mica fish indicators of non-coaxial deformation.

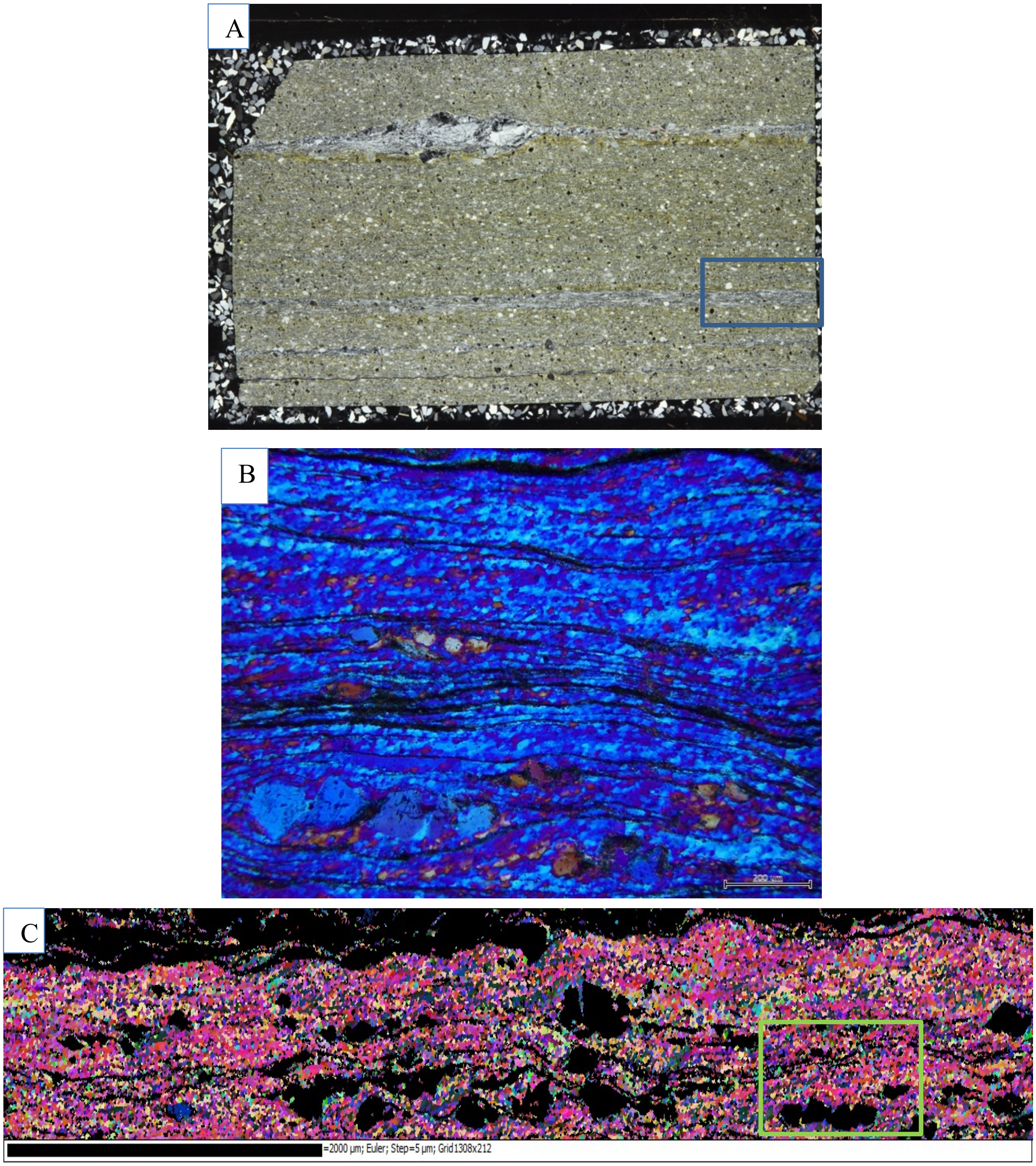

Figure 13. Sample C16-18-1. A. Picture of the thin section study area highlighted by the blue box. B. Small area that was examined under a gypsum plate, the location can be seen in C by the green box. C. C16-18-1 EBSD scan post extrapolation using a 5um step size.

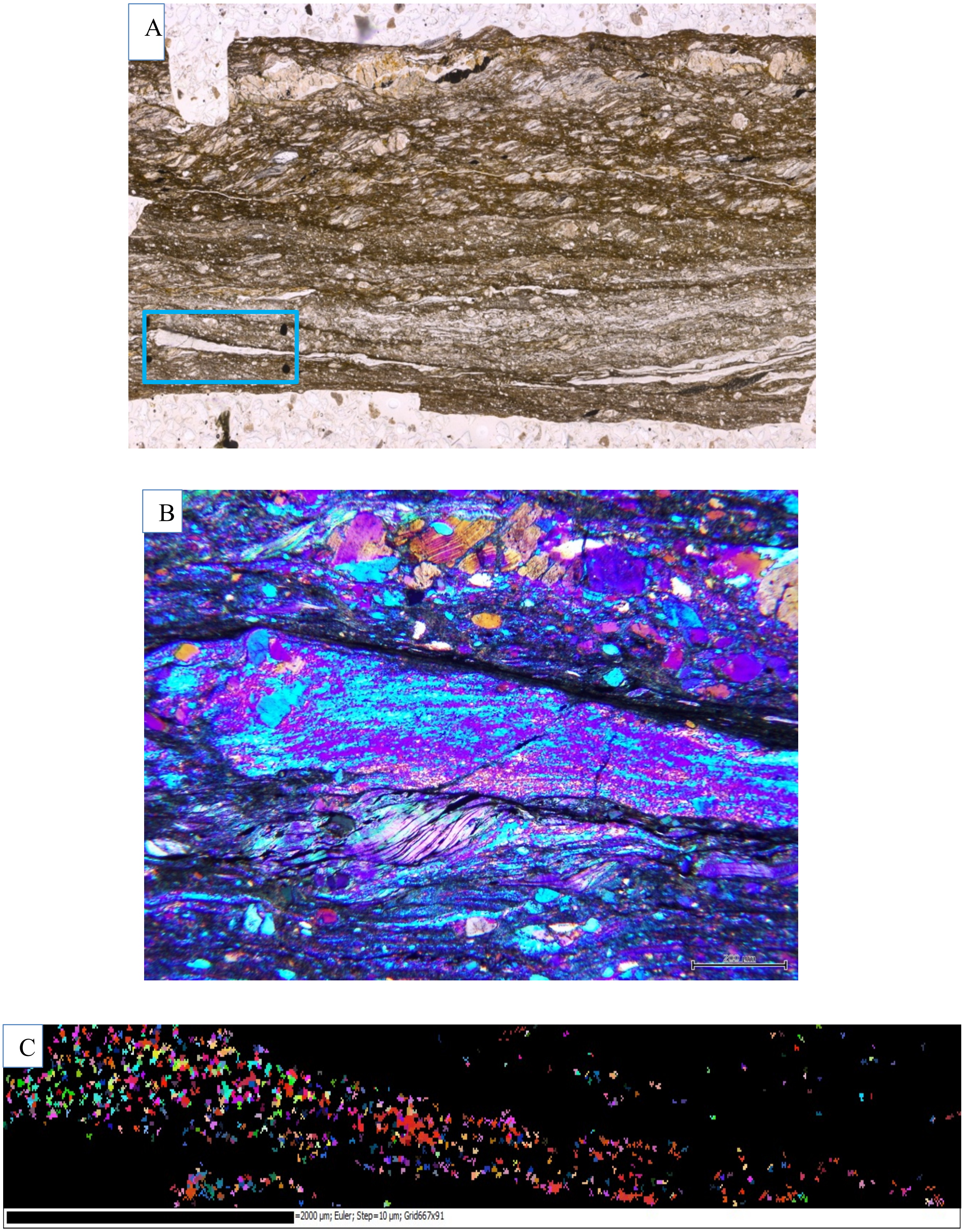

Figure 14. Sample C15-11-1. A. Entire thin section with study area highlighted by the blue box. B. Zoomed in to the blue box looking through a petrographic microscope with gypsum plate. C. C15-11-1 post extrapolation using a 10um step size.

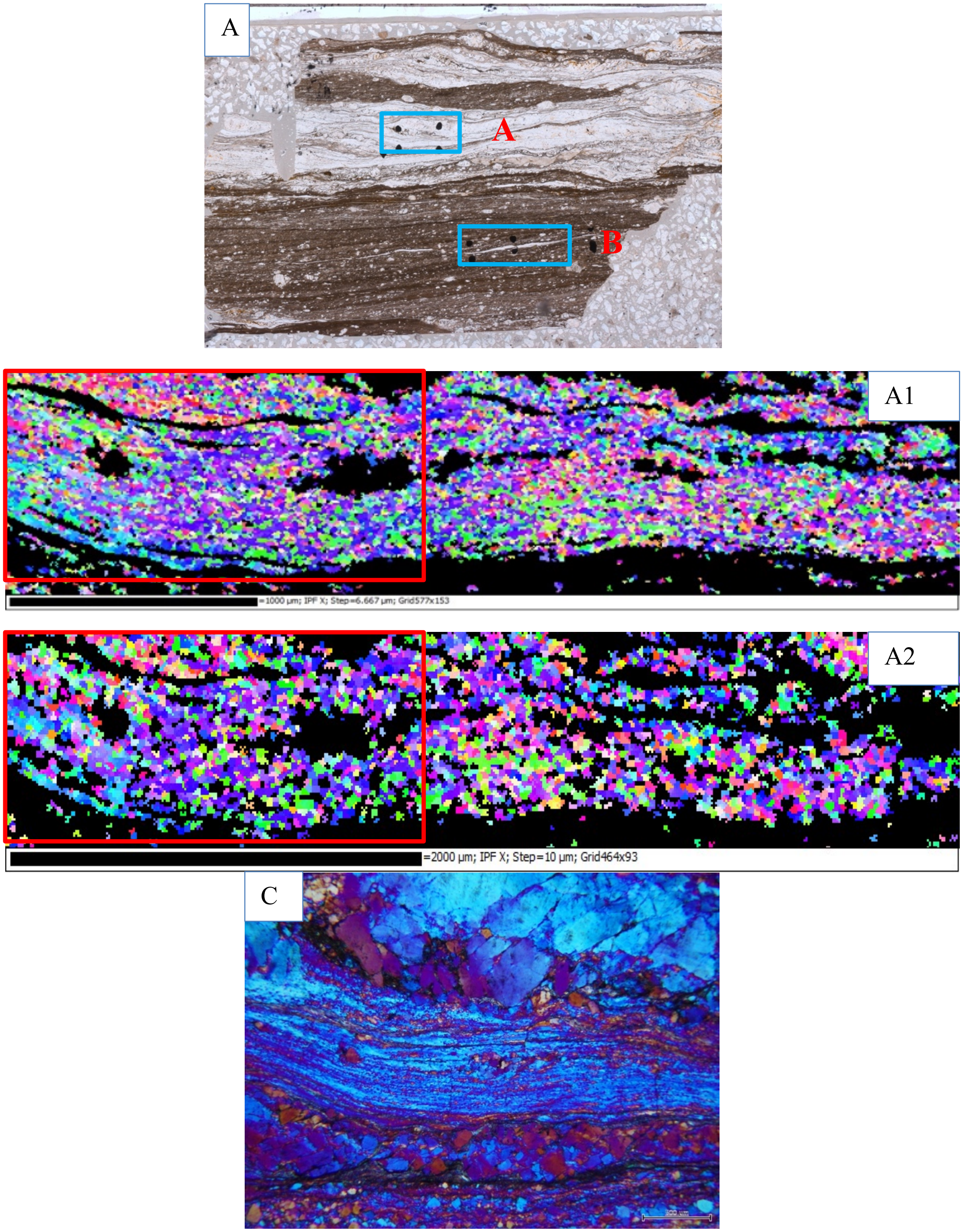

Figure 15. *Sample C15-17-2. A. The two-test area is highlighted by blue boxes. The upper area "A" will be referred to as C15-17-2, location A, and the lower section "B" will be referred to as C15-17-2, location B. A1. C15-17-2, location A, post extrapolation processed at a 5um step size. A2. C15-17-2, Location A, processed at a 10um step size. C. Petrographic view of this quartz vein under a gypsum plate. The approximate location of C can be seen in A1 and A2 by the red box.*

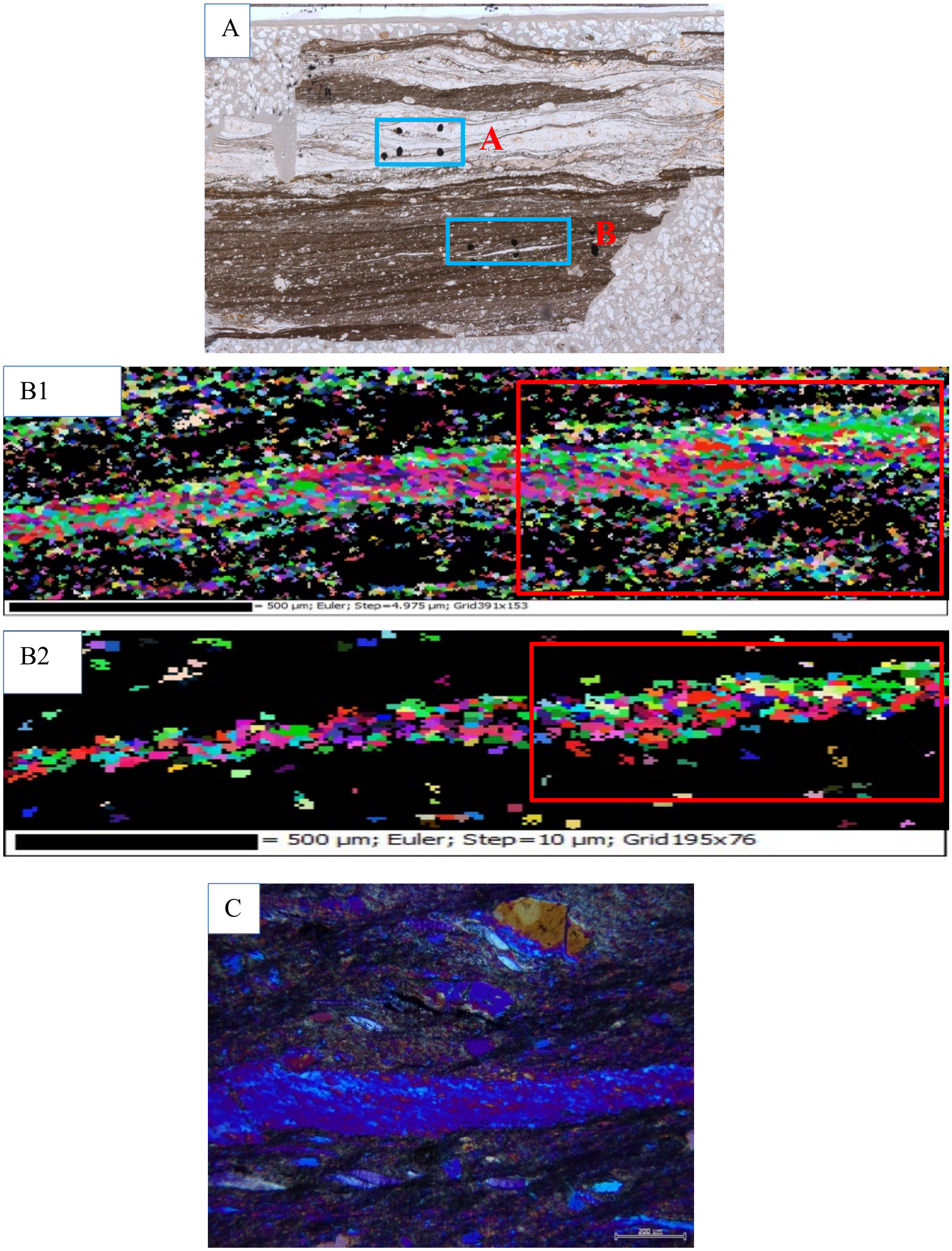

Figure 16. Sample C15-17-2, location B. A. The two-test area is highlighted by blue boxes. B1. C15-17-2, location B processed at a step size of 5um. B2. Location B processed at a step size of 10um. C. Petrographic view of this quartz vein under a gypsum plate. The approximate location of C can be seen in B1 and B2 by the red boxes. Note that C is flipped upside down when compared to B1 and B2.

Quartz c-axis Fabric Opening Angle Thermometry

The quartz c-axis fabric opening angles were used to determine the deformation temperature (Law, 2014). The quartz c-axis orientations were plotted on a contoured stereonet using Mtex (Figure 17). Using a protractor, the opening angle was measured from the stereonet x,y intersect. To measure the quartz c-axis orientations we looked for where their concentration along the edges of the stereonet was highest. Then the opening angles were plotted on Figure 18 to determine a deformation temperature. Sample C15-17-2, location A (both 5µm and 10µm), shows a CPO with a cross girdle fabric. This cross girdle yielded a quartz c-axis fabric opening angle of 65º which indicates a temperature of 510±50ºC (Law, 2014) (Figure 17&18). Sample C15-17-2, location B (both 5µm and 10µm step sizes), and sample C16-18-1, showed single girdle CPOs, which did not yield an opening angle. Sample C16-18-1 shows c-axis orientations that are extremely concentrated (Figure 17). The CPO for sample C15-11-1 exhibits a strong cross girdle fabric. This cross girdle had a clear c-axis fabric opening angle, which measured 50º, indicating a deformation temperature of 400±50ºC (Law, 2014) (Figure 17&18). Quartz c-axis CPO is nearly identical for areas analyzed at both a 5µm and 10µm step size. This shows that a 5µm step size is not essential for evaluation of CPOs and a 10µm will yield accurate CPO information.

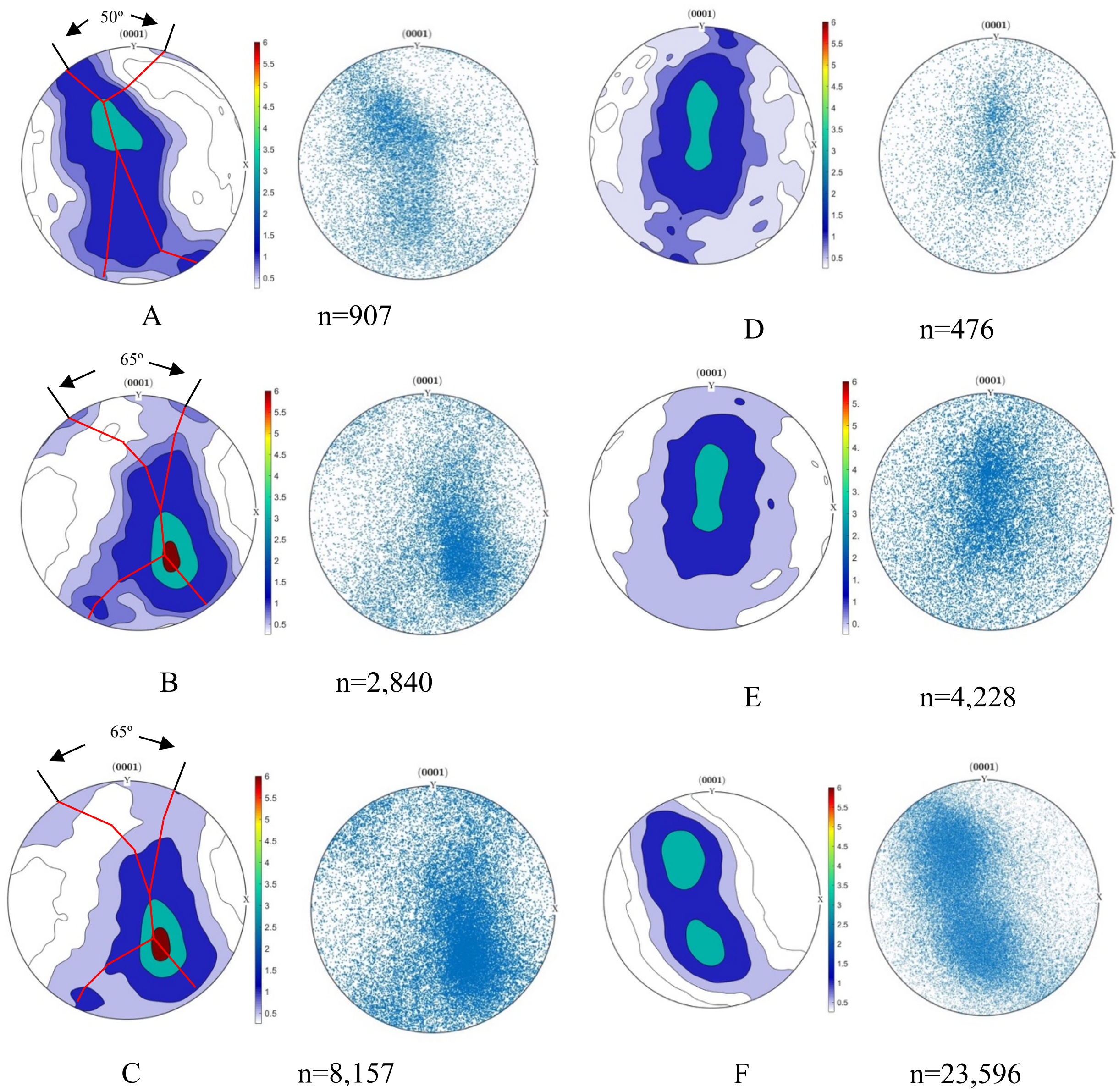

Figure 17. Stereographic projections of quartz c-axis orientations, both in contoured view and non-contoured. A. C15-11-1 had a quartz c-axis fabric opening angle of 50º and the temperature it yielded was 400±50ºC. B. C15-17-2 10µm, location A, had a quartz c-axis fabric opening angle of 65º this angle yielded a temperature of 500±50ºC. C. C15-17-2 5µm, Location A, had a quartz c-axis fabric opening angle of 65º which yielded a temperature of 500±50ºC. D. C15-17-2 10 µm, Location B, it was not possible to get a quartz c-axis fabric opening angle for this quartz vein. E. C15-17-2 5µm, Location B, it was not possible to get a quartz c-axis fabric opening angle for this quartz vein. F. C16-18-1, 5µm, this sample did not have a quartz c-axis fabric opening angle and it was not possible to obtain an opening angle. In A, B and C the red outline shows the fabric skeleton and the black arrows show the opening angle.

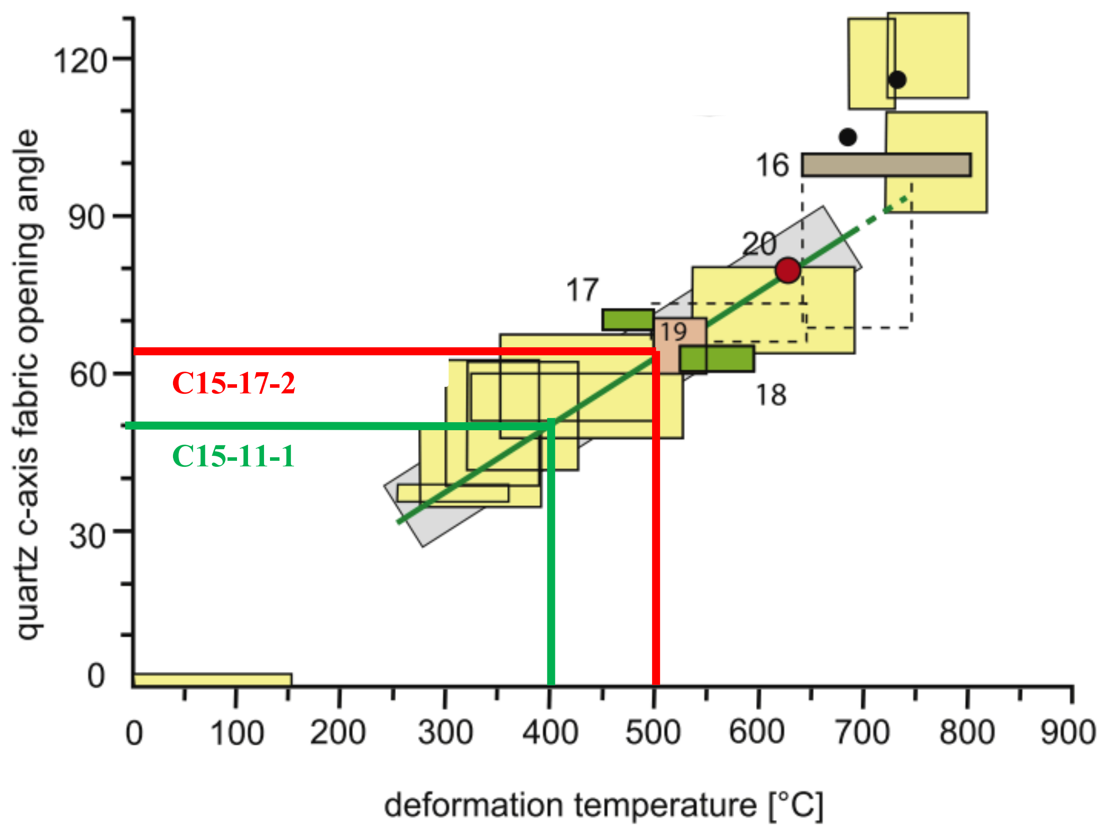

Figure 18. The red lines illistrage the temperatures obtained from the C15-17-2 which will not be used for this study. The green lines are the quartz c-axis fabric opening angle and the temperature derived from sample C15-11-1. (Figure altered by Chris Sargent based on Figure from Law, 2014)

Differential Stress and Grain Size Analysis

After post processing, a total of 40,402 quartz grains were identified among all of the samples. When comparing grain size of the same area at a 5µm and 10µm step size, there is a significant difference in the average grain diameters. The differential stress calculations are extremely sensitive to the grain size. For this reason, the higher resolution step size (5µm) will be used because those measurements are more accurate. The 5µm step size will give a more accurate representation of the overall grains. This will be discussed further in the discussion section. After removing the 10µm step size data, there were at total of 31,753 quartz grains among all the samples. The diameter was used to find to differential stress with Equation 1 (Holyoke and Kronenberg, 2010).

Sample C16-18-1 had a total of 23,596 quartz grains and an average grain diameter of 14.6µm with a standard deviation of 4.3 (Figure 19). The smallest grains had a diameter of 9.7µm and the largest had a diameter of 78.2µm. The differential stress calculated for this sample was 58.4MPa. Sample C15-17-2 5µm, location A, contained 8,147 quartz grains, an average grain diameter of 18.9µm and a standard deviation of 6.0 (Figure 20). The smallest grains had a dimeter of 13.0µm and the largest grains had a diameter of 108.5µm. The differential stress for this sample was 47.5 MPa. Sample C15-17-2 10µm, location A, had an average grain diameter of 30.4µm (Figure 21). Sample C15-17-2 5µm, location B, had a total of 4,228 grains and an average diameter of 14.1µm with a standard deviation of 4.0 (Figure 22). The smallest grains had a diameter of 9.7µm and the largest had a diameter of 74.1µm. The differential stress calculated for this sample was 60.12MPa. Sample C15-17-2 10µm, location B, had an average grain diameter of 25.1µm (Figure 23). Sample C15-11-1, 10µm, had an average grain diameter of 23.8µm (Figure 24). All samples that were analyzed at a 5µm step size show a better distribution of grain diameters and a better representation of total grain diameters.

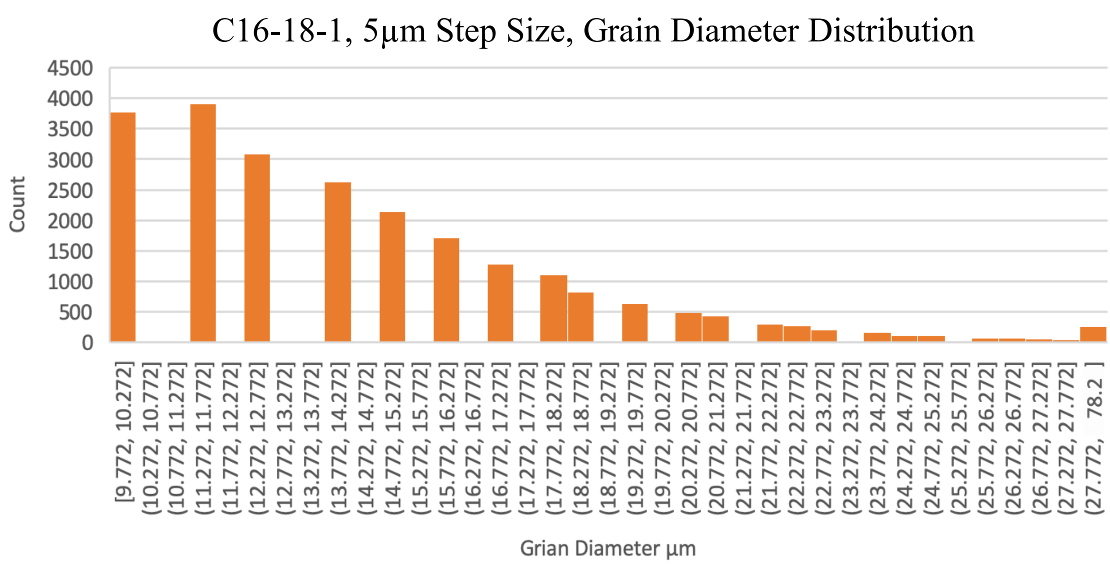

Figure 19. C16-18-1 quartz grain diameters analyzed at a 5 µm step size. Average grain diameter of 14.6µm.

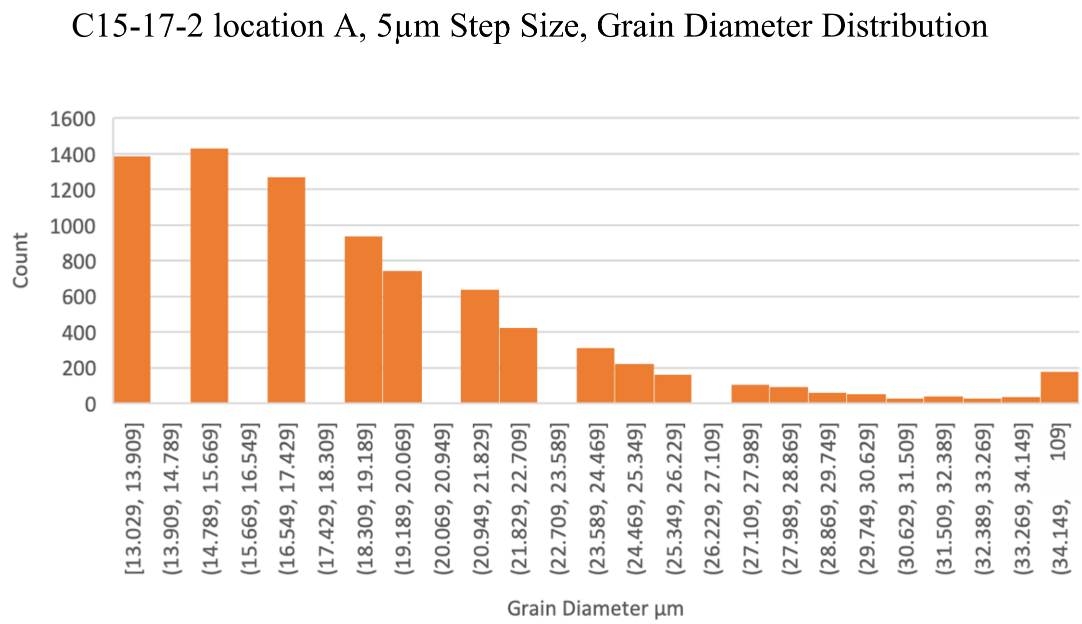

Figure 20.Sample C15-17-2, location A, quartz grain diameters analyzed at a 5 µm step size. Average grain diameter of 18.9µm.

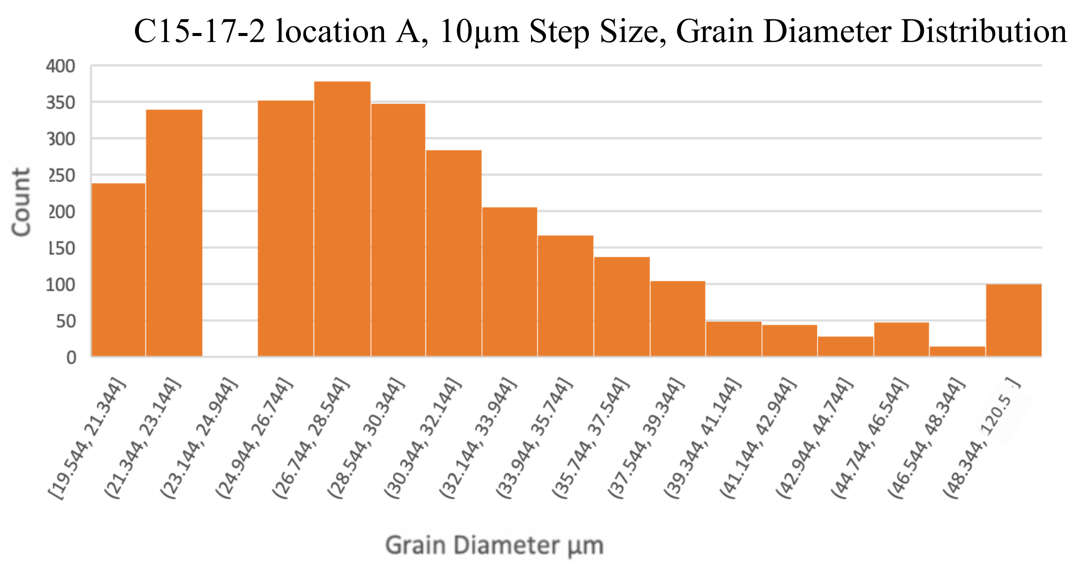

Figure 21.Sample C15-17-2, location A, quartz grain diameters analyzed at a 10 µm step size. Average grain diameter of 30.4µm.

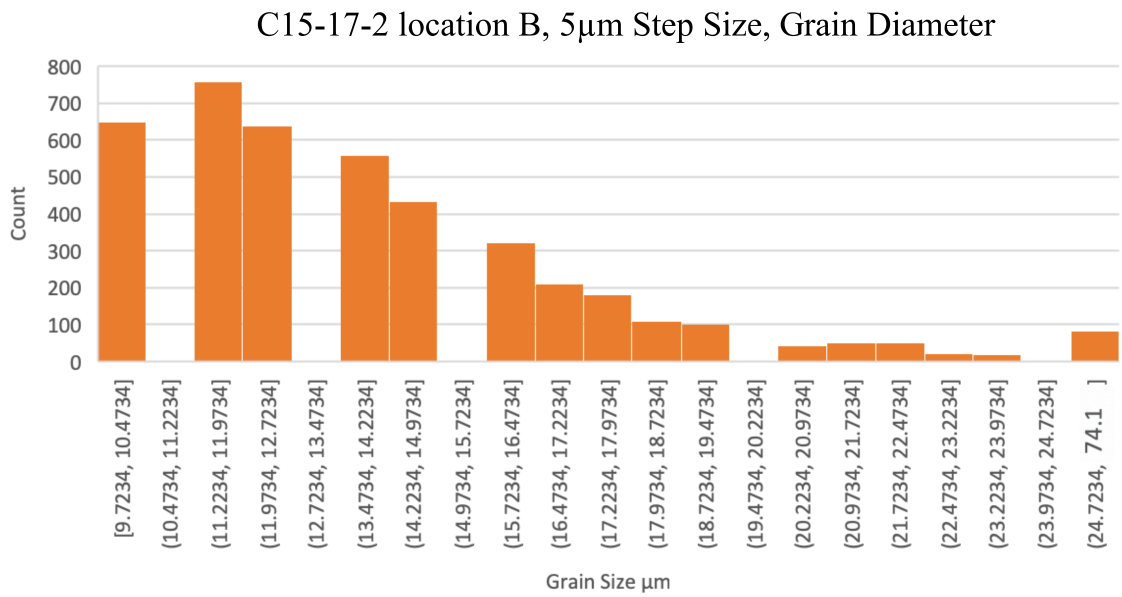

Figure 22. Sample C15-17-2, location B, quartz grain diameters analyzed at a 5µm step size. Average grain diameter of 14.1µm.

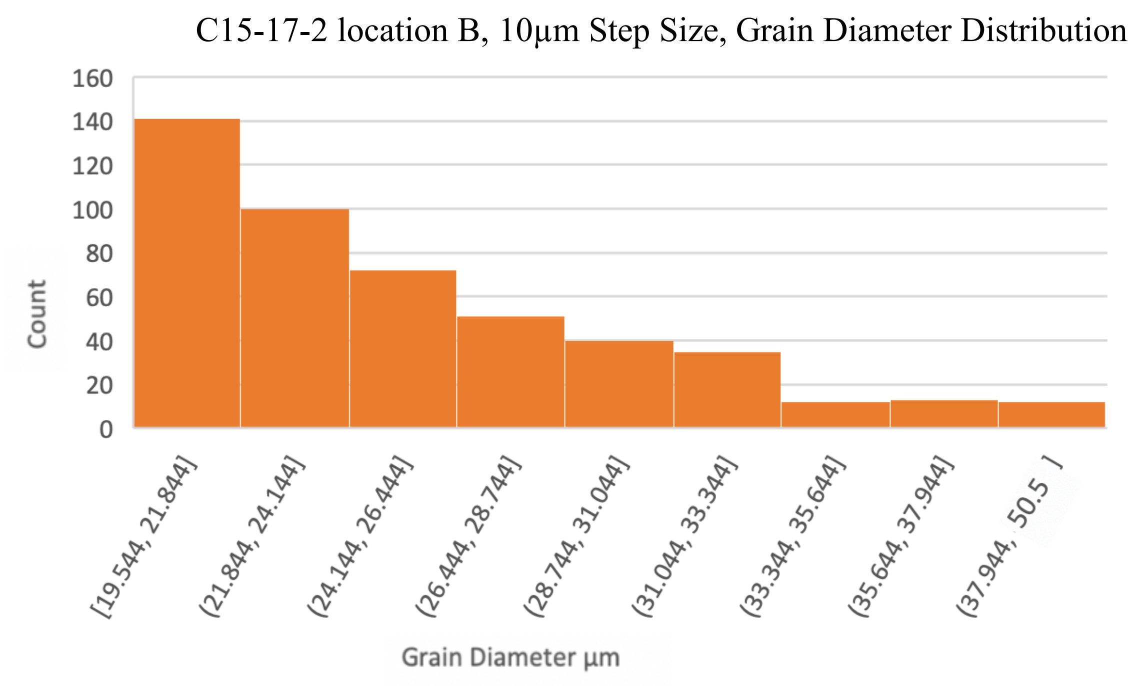

Figure 23. Sample C15-17-2, location B, quartz grain diameters analyzed at a 10µm step size. Average grain diameter of 25.1µm.

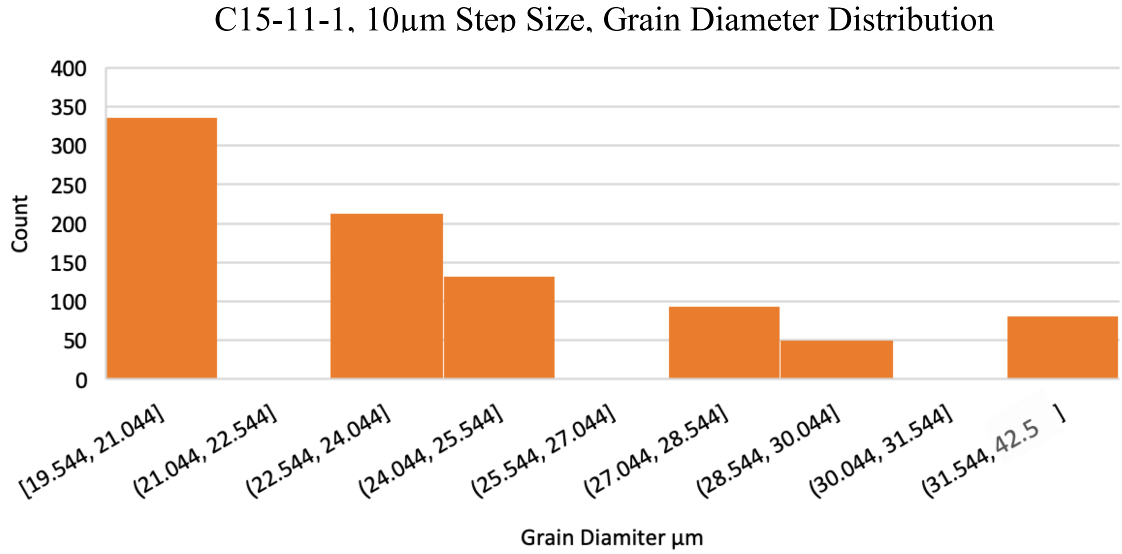

Figure 24. Sample C15-11-1, quartz grain diameters analyzed at a 10µm step size. Average grain diameter of 23.8µm.

Strain Rate

When determining strain rate, the quartz flow law equation was used (Equation 2). Within this equation there are many constants that were determined by Hirth et al (2001). The values that were not given included water fugacity, differential stress and temperature. Water fugacity f_{H_2O} was determined by using a fugacity calculator and has a unit of MPa (Withers). This calculation assumes a pressure of 0.5329 GPa and a depth of 20km. The 20km depth was based on the 400ºC deformation temperature and assuming that the depth would increase by 1km for every 20ºC. The temperature was determined using the quartz c-axis fabric opening angle and absolute temperature was found by converted into kelvin. The differential stress (σ) was found by using grain diameters calculations and Equation 1.

Each of the samples that were analyzed at a 5µm step size were calculated using five strain rate equations. The five stain equations were made to ensure that the range of strains rate included both the upper and lower givens for activation energy (Q) and material parameters (A). These numbers were not used to calculate the final deformation calculation rather to get an understanding of possible uncertainty. These calculations can be seen in Appendix A. Based on the middle A and Q values and the samples that were analyzed at a 5µm step size, it was possible to determine a strain rate for the Sandhill Corner shear zone. Sample C16-18-1 had a strain rate of $3.30x10^{-13}$ s^{-1}, sample C15-17-2, location B, had a strain rate of $3.73x10^{-13}$ s^{-1} and sample C15-17-2, location A, had a strain rate of $1.44x10^{-13}$ s^{-1} (Table 1).

Table 1. Values used for final deformation conditions calculations. Only samples that were analyzed at a 5µm step size. Grain size is average from each sample and differential stress is based on that average grain size. Temperature if based off the opening angle of C15-11-1. Strain rate based on the average A and Q values determined by Hirth et al. (2001) from Equation 1.

Sample	Grain Size (µm)	Temperature used in Calculations	Differential Stress (MPa)	Strain Rate (s^{-1})	Plate Velocity Meter/sec	Plate Velocity cm/year
C16-18-1	14.57	400º	58.40	$3.30x10^{-13}$	$3.31x10^{-10}$	1.04
C15-17-2 5um, Location B	14.03	400º	60.19	$3.73x10^{-13}$	$3.73x10^{-10}$	1.18
C15-17-2 5um, Location A	18.93	400º	47.45	$1.44x10^{-13}$	$1.44x10^{-10}$	0.45

Deformation

Plate Velocity

To find plate velocity, Equation 3 was used (Platt, 2015). The width, w assumes a constant 500m, this is based off on the width of the Sandhill Corner shear zone and the given measurement from Price at al. 2016. Strain rate, ε, was found using Equation 2 in the previous section. Equation 3 gives results in a velocity of meters per second, this was converted to centimeters per year in order to calculation the total deformation. The plate velocity was calculated using only the strain rates that were calculated from the middle A and Q values. All strain rate calculations that were made including the upper and lower limited can be seen in Appendix B. Sample C16-18-1, had a plate velocity of 1.04cm/year, sample C17-15-2, location B, had a plate velocity of 1.18cm/year and sample C15-17-2, location A, had a plate velocity of 0.45cm/year (Table 1).

Duration of Deformation

To find the duration of deformation in the Sandhill Corner shear zone we used the well-established regional cooling history developed by West and Hussey (2016) (Figure 25). This cooling history is based on $^{40}Ar/^{39}Ar$ thermochronology of hornblende, muscovite and biotite, as well as apatite fission track thermochronology. Based on the existing research done by Ludman et al. (1999) the Norumbega fault zone, and thus the Sandhill Corner shear zone, initiated around 370 Ma. Based on the deformation temperatures I have determined; the Sandhill Corner shear zone was active for approximately 30 million with the deformation ending around

340 million years ago. The quartz grains were constantly being deformed for these 30 million years, but around 340 million years ago the recrystallization ceased. The microstructures in this mylonite zone were continuously being overprinted during their time of deformation. Since the microstructures record of temperatures of 400±50ºC it shows that the shear zone stopped deforming when the regional temperature hit 400±50ºC which occurred around 340 Ma (Figure 25).

Total Displacement

Based on the plate velocity and the duration it was possible to calculate the total distance of deformation. The duration of deformation (30 Million years) was multiplied by the plate velocity (cm/years) and this an estimate of the total deformation in cm which was converted into kilometers. Total deformation ranged from 136km to 353km. Sample C16-18-1 yielded a distance of 313km, sample C15-17-2 location B, showed deformation of 353km and C15-17-2, location A, showed deformation of 136km. All calculations for displacement can be seen in Appendix C.

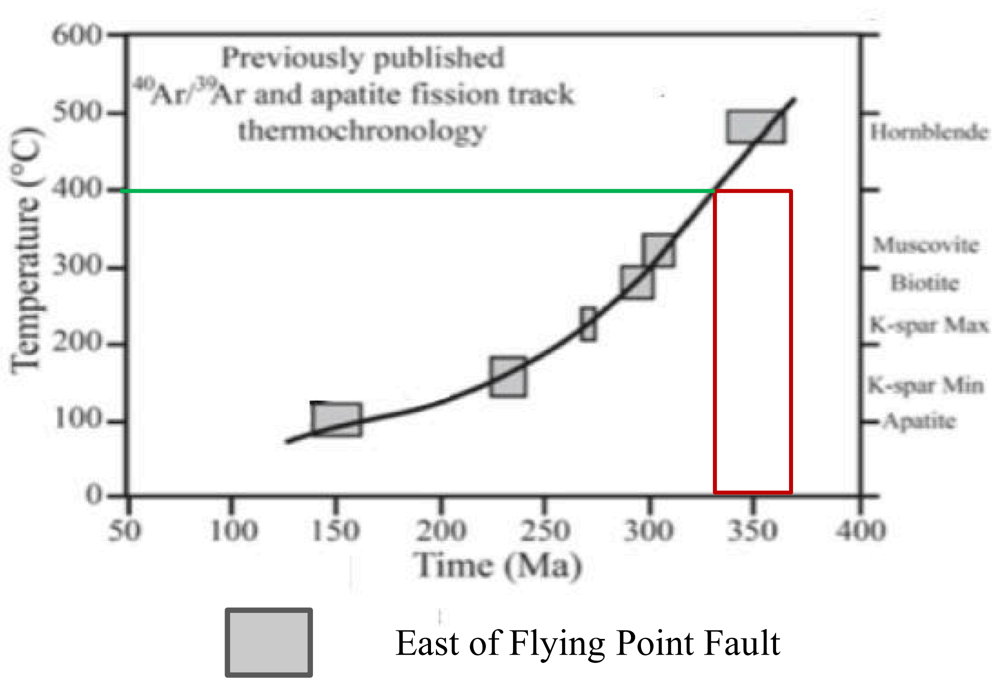

Figure 25. The duration of the Sandhill Corner shear zone. The starting age for the Norumbega at 370 million years is based on Ludman et al., (1999) and the end date of 340 million years is based on deformation ending when temperature reached 400±50ºC. The red box shows the time the fault system was active, and the green line shows the temperature that was the final deformation temperature. Modified from West et al. (1993), West and Hussey, (2016), West and Roden-Tice, (2003), West and Berry, (2016).

Discussion

Sources of Uncertainty

There are several sources of uncertainty that potentially affect our calculated shear zone displacements. First, Hirth et al. (2001) gives an uncertainty for the activation energy (Q) and the material parameter (A) based on the fitting of their experimental data. When these uncertainties are propagated to our calculations, they give a large range of potential strain rates. Although the upper and lower limits for Q and A give a large range of strain rates, the middle values (the best-fit of the experimental data) for these are likely the best values to use when calculating strain rate, though the true uncertainty is extremely large. Second, the width of the shear zone is extremely important to the displacement calculation. For the calculations in this study I used a width of 500m, but the shear zone varies from around 150-500m (Grover and Fernandes, 2003; West and Peterman, 2004). Mapping a mylonite zone boundary is potentially subjective, but in the case of the Sandhill Corner shear zone multiple mappers have agreed on the boundaries (Grover and Fernandes, 200; West and Peterman, 2004.). Our simplifying assumption of a 500m wide shear zone is in broad agreement with existing maps and literature. Finally, the total duration of deformation constitutes a major uncertainty in these calculations, which we discuss in detail below.

Evaluating Temperature form CPO

The crystallographic preferred orientation (CPO) was used to approximate the recrystallization temperature of the quartz microstructures. The CPO patterns are a result of rotating crystallographic orientation during deformation and form because of intracrystalline slip (Fossen, 2016). The crystalline lattice of quartz can deform in various directions, known as slip systems, which will cause the potential for the CPO to form girdles (Figure 17). The deformation temperature is calculated using the quartz c-axis fabric opening angle from sample C15-11-1 and this sample was analyzed at a step size of 10μm. When examining CPOs, the samples that were analyzed at a 10μm and 5μm step size showed the same slip systems and opening angles (Figure 17). For this reason, we can be confident that the low-resolution data still gives us good c-axis fabric information for sample C15-11-1. When plotted, these pole figures can either form a single girdle or a cross girdle. The orientations of these girdles will be determined by the dislocation creep which reflects the activity of various slip systems (Fossen, 2016 p. 251). The samples analyzed in this study resulted in both a cross girdle and a single girdle (Figure 17). Samples C15-11-1 and C15-17-2 (location A), both had cross girdles which would indicate that Basal<a>, Rhomb <a> and Prism <a> slip all occurred. Sample C15-17-2 (location B) did not result in a cross girdle and it would appear that Prism <a> was the most active slip system. Sample, C16-18-1, had a single girdle and it appeared that Rhomb <a> slip occurred (Fossen, 2016). These CPO slip systems are in line with the findings of Price et al. (2016) who suggested that the quartz CPO patterns in the Sandhill Corner shear zone were mostly dominated by prism<a>, rhomb <a> and also basal <a>.

The temperature found from the quartz c-axis fabric opening angles varied between 400±50ºC to 500±50ºC. Based on the knowledge of quartz in the Sandhill Corner shear zone, and the slip systems of our quartz veins, the 500±50ºC temperature is unlikely to be a meaning estimate of the recrystallization temperature (West and Hubbard, 1997; Fossen, 2016; Price et al. 2016). Based on the 50º quartz c-axis fabric opening angle it was possible to find a 400±50ºC recrystallization temperature. When Basal<a>, Rhomb <a> and Prism <a> slip are present it is usually an indicator deformation occurred around 300-400ºC and when just Rhomb <a> and Prism <a> are dominant it is an indicator of deformation temperature slightly above 400ºC (Fossen, 2016). These slip systems help to show that the estimated 400±50ºC is likely an accurate deformation temperature. Although on the lower end of deformation temperature, the a 400±50ºC based on these samples is in line with the existing research that has been done in this area. The common deformation temperature in quartz associated with BLG is between 280-400ºC and SGR is between 400-500ºC which further supports our temperature of a 400±50ºC (Stipp et al, 2002). Based on muscovite samples within the Sandhill Corner, West and Lux find a closure temperature of ~320ºC indicating that the quartz deformation temperature would have been greater than that 320ºC (West and Lux, 1993). The brittle deformation in feldspar porphyroclasts also an indicator that the temperature of deformation was less than 500ºC (West and Lux, 1993; Stipp et al., 2010). All previous work and the observed quartz microstructures are consistent with deformation temperatures of 400±50ºC, for this reason this temperature was used in strain rate calculations.

Evaluating Grain Size Measurements

The grain sizes varied significantly between samples and this change is expected because each quartz vein is different. However, calculated grain sizes for the same analytical area were different when using a pixel 10μm and 5μm step size. Samples that were analyzed at both of the step sizes showed that average grain sizes with the 5μm step size were smaller by at least 10μm, when they should be identical. This causes some concern on the data coming from the 10μm step size. The 5μm step size data is a much higher resolution, so we consider these data to provide a much more accurate representation of the true grain size in the sample. The samples analyzed with 10μm step sizes were not used to calculate, differential stresses or the total distance of displacement. The average calculated grain sizes fall within the expected range for BLG and the SGR, which supports the accuracy of the grain measurements (Stipp et al., 2010; Law, 2014).

Plate Velocity

When calculating the plate velocity, the middle A and Q values from Equation 2 were used. These middle values are best fit values for the flow law equation derived by Hirth et al. (2001). In addition, these middle values yielded plate velocities that aligned with existing literature which reinforces the confidence in these values. While using the middle A and Q values the plate velocity calculations are between 0.45-1.18 cm/year. Using combinations of both upper and lower limits of A and Q values, this range widened to between 0.005-68.38 cm/year. The range of plate velocities when using the upper and lower limits of A and Q are not realistic and it appears that the best values to use are the middle A and Q values. The three plate velocities found in this study were, 0.45cm/year, 1.04cm/year and 1.18cm/year. The velocities found in this study fall within this range of existing literature and this adds confidence to these calculations (Platt, 2015; Kuiper, 2016; Kuiper and Wakabayashi, 2018). These velocities were also calculated using a given width of 500m. These plate velocities are on the slower side compared to various plates that are moving around today (Syracuse et al., 2010). When compared to the San Andreas Fault System (SAFS), the NFS is moving slower than the SAFS. The SAFS is moving around 2-4cm/year, two or four times as fast as the NFS (Kuiper, 2016; Kuiper and Wakabayashi, 2018). The plate velocities of 1.04 and 1.18cm/year are consistent with prevision work done on faults around the world.

Displacement Estimates

The calculated displacement distances of the Sandhill Corner shear zone are 136km, 313km, and 353km, with an average displacement of 267km. These distances are relatively consistent resulting from successful calculations. These distances were based on using a deformation duration of 30 million years. This time assumes recrystallization beginning 370 Ma and ending around 340 Ma based on the well-constrained regional cooling curve from West and Hussey, 2016. This is the best available estimate of the time period the fault was active because this recrystallization period was the last metamorphic period. We know this because there are no indicators of overprinting deformation after 400±50ºC. In our calculation we have assumed constant plate velocity since 370 Ma. During time of deformation the plate velocity likely fluctuated. This assumption of constant velocity would have alerted the overall displacement because it does not account for a changing velocity. In this study, we assumed a 30 Ma period of deformation. If the duration was shorter or longer it would significant change the total displacement. Other studies suggest that the deformation may have lasted longer than 30 Ma, which would produce a larger total displacement. Our data only provided an estimate for the parts of the shear zone that record these microstructures. Previous studies have suggested that the Sandhill Corner shear zone was active until as late at 290 Ma (West and Lux, 1993). If deformation continued in a narrower part of the shear zone (Price et al., 2016) where we have not analyzed samples then our data are still constant with longer duration of deformation. If significant deformation continued after our quartz recrystallization microstructure were recorded our displacement estimates would be a minimum.

There is a large variety of displacement measurements that have been that have previously been proposed for the NFS, many of which are inconsistent with one another. The methods for these estimates also vary greatly, they include, offsets of $^{40}Ar/^{39}Ar$ thermochronology patterns, offset of plutons, shear strain and CPO. Hubbard (1999), reviewing extensive existing literature for the Maritime Appalachians, found that the displacement of the NFS was between 100km to 500km. West and Lux (1993) used offset patterns in the regional thermochronology to find that there was around 30km of displacement. With about 100 citations, West and Lux (1993) appear to have the most widely accepted displacement value. Ludman et al. (1999) used pluton displacement to argue that displacement is likely around 60km but there could have been as much as 1900km of dextral displacement. Swanson (1999) using shear strain estimates for deformed granites suggests that the displacement could have fallen in the 100-150km range. Price et al. (2016) compares the findings of Hubbard (1999), Swanson (1999), Wang and Ludman (2004) to show a wide range of possible displacement occurring between 25-300km. The displacements that were found in this study are on the high end when compared to previous work but are within the range of known displacements.

It is also useful to compare my estimates to offsets determined for other shear zones. A compilation of displacement estimates is shown in Figure 26 (Fossen, 2016). It is clear that the estimated displacement of the NFS are reasonable when compared to other fault and shear zones (Figure 26) (Fossen 2016). This figure shows that it is indeed likely that in a shear zone with a width of 500m total displacement is greater than 100km. It is clear that with the quartz grain sizes that were measured it is likely that the displacement was well above 100km and could have likely fallen between the 100-350km. This study provides an independent method for estimating displacement. The estimates given here are in greater agreement with the higher end of existing estimates (100-500 km) rather than the low end (30-60 km).

When compared to the San Andreas Fault System, which is often considered a similar fault system, the plate velocity across the NFS appears to be relatively slow. However, based on existing knowledge on plate velocities it seems unlikely that these distances would only be around 30km. The strain rate and temperature calculated from these samples fall within the appropriate range of 10^{-12} to 10^{-14} S^{-1} and 280-500ºc (Price at al., 2016). With the strain rates falling within the appropriate range, according to popular literature, and the added confidence of removing the 10um step size measurements, it is possible to say that a displacement between 136km – 356km is an accurate representation for the Sandhill Corner shear zone and potentially the Norumbega fault system.

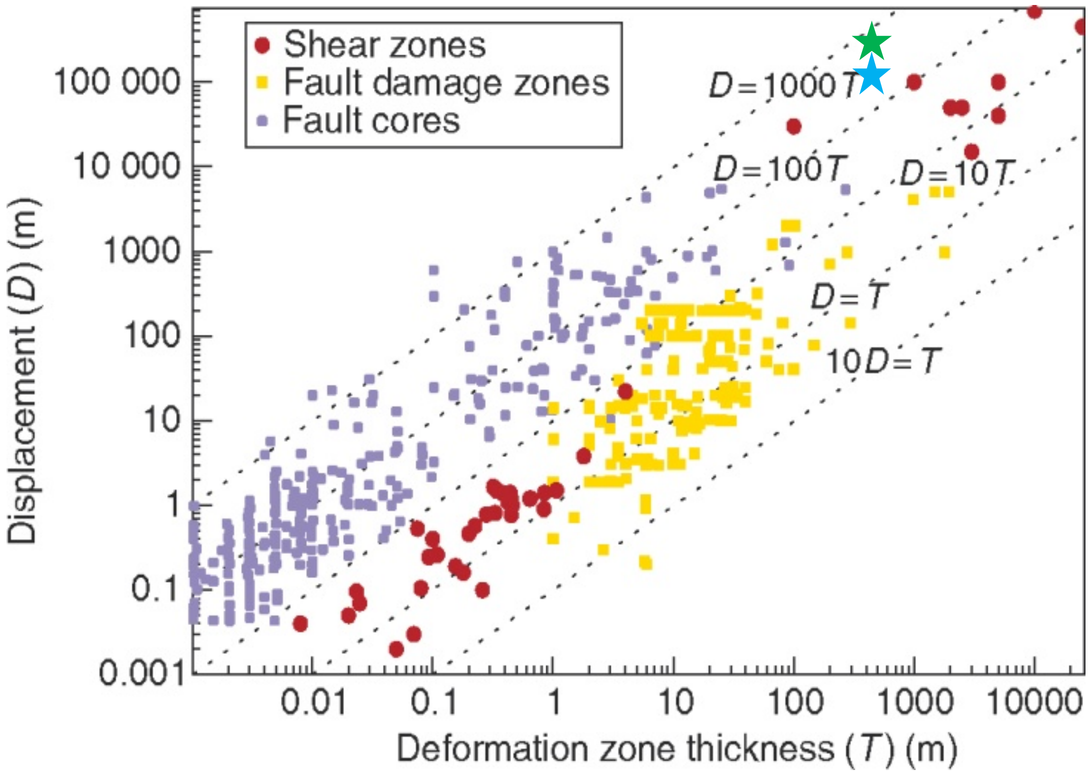

Figure 26. Deformation Zone thickness plotted against the Displacement. The values calculated in this study fall within the upper range and are closely related to other shear zone displacements. The blue star is the value representing the 136km of displacement and the green star represents the 313 and 353km displacement values. All other data are based off of Fossen, 2016.

Conclusion

The Sandhill Corner is a low-medium grade mylonitazion zone, which underwent deformation around 400±50ºC. The quartz grains indicated BLG and SGR deformation mechanisms. In select samples the quartz c-axis fabric opening angle showed strong cross girdles which yielded a deformation temperature of 400±50ºC. Average grain diameters ranged between 14.03-18.93μm and helped to calculated differential stress values between 47.5MPa 60.1MPa. Strain rates ranged between $1.44x10^{-13}s^{-1}$ and $3.73x10^{-13}s^{-1}$. The kinematic indicators observed during this study are consistent with previous observations of dextral kinematics. These include brittle feldspar deformation, mica fish and porphyroclasts. The plate velocities, ranging between .45-1.18cm/year, are in line with other velocities that have been recorded in similar faults around the world. Duration lasted for 30 million years and the deformation concluded around 340 Ma. The duration is the largest uncertainty in this study and studies suggest that duration possibly lasted until 290 Ma. If deformation continued after our deformation ends date (340 Ma) then our displacement estimates would be a minimum. The total displacement calculated for the Sandhill Corner shear zone was between 136-353km. There is a wide variety of displacement estimates for the NFS which stems from the variety of methods used. The quartz CPO method and the displacement estimates found in this study will help to provide a more precise estimate for total displacement. Future work that combines thermochronology with deformation microstructures might lead to a more consistent estimate of total displacement.

References

Bothner, W. A., and Hussey , A. M., 1999, Norumbega connections: Casoc Bay, Maine, to Massachusetts: Special Paper of the Geological Society of America, v. 331, p. 59-72.

David P. West, J. and Hussey, A. M., 2016, Middle Ordovician to Early Silurian Terranes of the Northern Casco Bay Region, Maine: New England Intercollegiate Geological Conference, p. 249-266.

F. Bachmann, R. H. a. H. S., 2010, Texture Analysis with MTEX – Free and Open Source Software Toolbox no. 160, p. 63-68.

Fossen, H., 2016, Structural geology, Cambridge, United Kingdom, Cambridge University Press, 510 p.:

Grover, T.W., Fernandes, L.C., 2003. Bedrock geology of the Weeks Mills 7.5′ quadrangle, Maine. Maine Geological Survey Open-File Maps 03-49, Scale = 1:24,000.

Henry N. Berry IV and David P. West, J., 2016, Guidebook for Field Trips along the Maine Coast from Maquoit Bay to Muscongus Bay; New England Intercollegiate Geological Conference 108th Annual Meeting: New England Intercollegiate Geological Conference.

Hirth, G., Teyssier, C., and Dunlap, J. W., 2001, An evaluation of quartzite flow laws based on comparisons between experimentally and naturally deformed rocks: International Journal of Earth Sciences, v. 90, no. 1, p. 77-87.

Holyoke, C. W., and Kronenberg, A. K., 2010, Accurate differential stress measurement using the molten salt cell and solid salt assemblies in the Griggs apparatus with applications to strength, piezometers and rheology: Tectonophysics, v. 494, no. 1, p. 17-31.

Hubbard, M. S., 1999, Norumbega fault zone: Part of an orogen-parallel strike-slip system, northern Appalachians: Geological Society of America Special Papers, v. 331, p. 155-165.

Kuiper, Y. D., 2016, Development of the Norumbega fault system in mid-Paleozoic New England, USA: An integrated subducted oceanic ridge model: Geology, v. 44, no. 6, p. 455-458.

Kuiper, Y. D., and Wakabayashi, J., 2018, A comparison between mid-Paleozoic New England, USA, and the modern western USA: Subduction of an oceanic ridge-transform fault system: Tectonophysics, v. 745, p. 278-292.

Law, R. D., 2014, Deformation thermometry based on quartz c-axis fabrics and recrystallization microstructures: A review: Journal of Structural Geology, v. 66, p. 129-161.

Ludman, A., Lanzirotti, A., Lux, D., and Chunzeng, W., 1999, Constraints on timing and displacement of multistage shearing in the Norumbega fault system, eastern Maine: Geological Society of America Special Papers, v. 331, p. 179-194.

Maine Geologcial Survey, 2019, Maine Bedrock 100k Map: Maine Agriculture Conservation and Forestry.

Passchier, C. W., and Trouw, R. A. J., 2005, Microtectonics, New York;Berlin;, Springer, 366 p.:

Platt, J. P., 2015, Influence of shear heating on microstructurally defined plate boundary shear zones: Journal of Structural Geology, v. 79, p. 80-89.

Price, N. A., Johnson, S. E., Gerbi, C. C., and West, D. P., 2012, Identifying deformed pseudotachylyte and its influence on the strength and evolution of a crustal shear zone at the base of the seismogenic zone: Tectonophysics, v. 518-521, p. 63-83.

Price, N. A., Song, W. J., Johnson, S. E., Gerbi, C. C., Beane, R. J., and West, D. P., 2016, Recrystallization fabrics of sheared quartz veins with a strong pre-existing crystallographic preferred orientation from a seismogenic shear zone: Tectonophysics, v. 682, p. 214-236.

Syracuse, E. M., van Keken, P. E., and Abers, G. A., 2010, The global range of subduction zone thermal models: Physics of the Earth and Planetary Interiors, v. 183, no. 1-2, p. 73-90

Schmidt, N.-H., and Olesen, N.O., 1989, Computer Aided Determination of Crystal-Lattice Orientations from Electron Channeling Patterns in the SEM: Canadian Mineralogist, v. 27, 15-22.

Schwartz, A. J., 2009, Electron backscatter diffraction in materials science, New York, NY, Springer Science+Business Media, 403 p.:

Stipp, M., Stünitz, H., Heilbronner, R., and Schmid, S. M., 2002, The eastern Tonale fault zone: a 'natural laboratory' for crystal plastic deformation of quartz over a temperature range from 250 to 700 °C: Journal of Structural Geology, v. 24, no. 12, p. 1861-1884.

Stipp, M., and Tullis, J., 2003, The recrystallized grain size piezometer for quartz: Geophysical Research Letters, v. 30, no. 21, p. 2088.

Stipp, M., Tullis, J., Scherwath, M., and Behrmann, J. H., 2010, A new perspective on paleopiezometry: Dynamically recrystallized grain size distributions indicate mechanism changes: Geology, v. 38, no. 8, p. 759-762.

Swanson, M. T., 1999, Dextral transpression at the Casco Bay restraining bend, Norumbega fault zone, coastal Maine: Geological Society of America Special Papers, v. 331, p. 85-104.

Swapp, S., 2019, Electron Backscatter Diffraction (EBSD), University of Wyoming, Volume 2019: Integrating Research and Education

Wang, C., and Ludman, A., 2004, Deformation conditions, kinematics, and displacement history of shallow crustal ductile shearing in the Norumbega fault system in the Northern Appalachians, eastern Maine: Tectonophysics, v. 384, no. 1, p. 129-148.

West, D. P., and Hubbard, M. S., 1997, Progressive localization of deformation during exhumation of a major strike-slip shear zone: Norumbega fault zone, south-central Maine, USA: Tectonophysics, v. 273, no. 3-4, p. 185-201.

West, D. P., Jr., Lux, D. R, and Hussey, A. M., 1993, Contrasting thermal histories across the Flying Point fault, Maine: Evidence for Mesozoic displacement: Geological Society of America Bulletin, v. 105, p. 1478-1490.

West, D. P., and Lux, D. R., 1993, Dating mylonitic deformation by the 40Ar- 39Ar method: An example from the Norumbega Fault Zone, Maine: Earth and Planetary Science Letters, v. 120, no. 3, p. 221-237.

West, D.P., Jr., Peterman, E.M., 2004. Bedrock Geology of the Razorville 7.5′ quadrangle, Maine. Maine Geological Survey Open-File Maps 04-29: Scale = 1:24,000.

West Jr, D. P., and Roden-Tice, M. K., 2003, Late Cretaceous reactivation of the Norumbega fault zone, Maine: Evidence from apatite fission-track ages: Geology, v. 31, no. 7, p. 649-652.

Withers, T., Fugacity Calculator, Volume 2019: National Science Foundation and the University of Minnesota.https://www.esci.umn.edu/people/researchers/withe012/fugacity.htm

Appendix A: All Calculations for Stress and Strain Rate

Sample and A & Q Values		Sample Temp	Temp in K	Fugacity Value	Stress		Strain
-A-Q							
C15-11-1		400	673	135.49	39.56		8.8445E-13
C16-18-1		400	673	135.49	58.40		4.20328E-12
C15-17-2 Location B 5um		400	673	135.49	60.20		4.74376E-12
C15-17-2 Location B 10um		400	673	135.49	37.97		7.50833E-13
C15-17-2 Location A 5um		400	673	135.49	47.45		1.83209E-12
C15-17-2 Locaiton A 10um		400	673	135.49	32.30		3.93223E-13
Average							2.1346E-12
-A+Q							
C15-11-1		400	673	135.49	39.56		4.15098E-15
C16-18-1		400	673	135.49	58.40		1.97272E-14
C15-17-2 Location B 5um		400	673	135.49	60.20		2.22638E-14
C15-17-2 Location B 10um		400	673	135.49	37.97		3.52387E-15
C15-17-2 Location A 5um		400	673	135.49	47.45		8.5985E-15
C15-17-2 Locaiton A 10um		400	673	135.49	32.30		1.84551E-15
Average							1.00183E-14
Middle A Middle Q							
C15-11-1		400	673	135.49	39.56		2.07098E-13
C16-18-1		400	673	135.49	58.40		3.30618E-13
C15-17-2 Location B 5um		400	673	135.49	60.20		3.73131E-13
C15-17-2 Location B 10um		400	673	135.49	37.97		5.90584E-14
C15-17-2 Location A 5um		400	673	135.49	47.45		1.44107E-13
C15-17-2 Locaiton A 10um		400	673	135.49	32.30		3.09298E-14
Average							1.90824E-13
+A-Q							
C15-11-1		400	673	135.49	39.56		4.04272E-12
C16-18-1		400	673	135.49	58.40		1.92127E-11
C15-17-2 Location B 5um		400	673	135.49	60.20		2.16832E-11
C15-17-2 Location B 10um		400	673	135.49	37.97		3.43197E-12
C15-17-2 Location A 5um		400	673	135.49	47.45		8.37424E-12
C15-17-2 Locaiton A 10um		400	673	135.49	32.30		1.79737E-12
Average							9.75702E-12
+A+Q							
C15-11-1		400	673	135.49	39.56		1.89736E-14
C16-18-1		400	673	135.49	58.40		9.01707E-14
C15-17-2 Location B 5um		400	673	135.49	60.20		1.01765E-13
C15-17-2 Location B 10um		400	673	135.49	37.97		1.61072E-14
C15-17-2 Location A 5um		400	673	135.49	47.45		3.93027E-14
C15-17-2 Locaiton A 10um		400	673	135.49	32.30		8.4356E-15
Average							4.57925E-14

Appendix B: All Calculations for Plate Velocity

Sample and A & Q Values	Width (Meters)	Strain Rate		Velovity (m/second)	Velocity (cm/year)
-A-Q					
C15-11-1	500	8.8445E-13		8.8E-10	2.8E+00
C16-18-1	500	4.20328E-12		4.2E-09	1.3E+01
C15-17-2 Location B 5um	500	4.74376E-12		4.7E-09	1.5E+01
C15-17-2 Location B 10um	500	7.50833E-13		7.5E-10	2.4E+00
C15-17-2 Location A 5um	500	1.83209E-12		1.8E-09	5.8E+00
C15-17-2 Locaiton A 10um	500	3.93223E-13		3.9E-10	1.2E+00
Average	500	2.1346E-12		2.1E-09	6.7E+00
-A+Q					
C15-11-1	500	4.15098E-15		4.2E-12	1.3E-02
C16-18-1	500	1.97272E-14		2.0E-11	6.2E-02
C15-17-2 Location B 5um	500	2.22638E-14		2.2E-11	7.0E-02
C15-17-2 Location B 10um	500	3.52387E-15		3.5E-12	1.1E-02
C15-17-2 Location A 5um	500	8.5985E-15		8.6E-12	2.7E-02
C15-17-2 Locaiton A 10um	500	1.84551E-15		1.8E-12	5.8E-03
Average	500	1.00183E-14		1.0E-11	3.2E-02
Middle A Middle Q					
C15-11-1	500	2.07098E-13		2.1E-10	6.5E-01
C16-18-1	500	3.30618E-13		3.3E-10	1.0E+00
C15-17-2 Location B 5um	500	3.73131E-13		3.7E-10	1.2E+00
C15-17-2 Location B 10um	500	5.90584E-14		5.9E-11	1.9E-01
C15-17-2 Location A 5um	500	1.44107E-13		1.4E-10	4.5E-01
C15-17-2 Locaiton A 10um	500	3.09298E-14		3.1E-11	9.8E-02
Average	500	1.90824E-13		1.9E-10	6.0E-01
+A-Q					
C15-11-1	500	4.04272E-12		4.0E-09	1.3E+01
C16-18-1	500	1.92127E-11		1.9E-08	6.1E+01
C15-17-2 Location B 5um	500	2.16832E-11		2.2E-08	6.8E+01
C15-17-2 Location B 10um	500	3.43197E-12		3.4E-09	1.1E+01
C15-17-2 Location A 5um	500	8.37424E-12		8.4E-09	2.6E+01
C15-17-2 Locaiton A 10um	500	1.79737E-12		1.8E-09	5.7E+00
Average	500	9.75702E-12		9.8E-09	3.1E+01
+A+Q					
C15-11-1	500	1.89736E-14		1.9E-11	6.0E-02
C16-18-1	500	9.01707E-14		9.0E-11	2.8E-01
C15-17-2 Location B 5um	500	1.01765E-13		1.0E-10	3.2E-01
C15-17-2 Location B 10um	500	1.61072E-14		1.6E-11	5.1E-02
C15-17-2 Location A 5um	500	3.93027E-14		3.9E-11	1.2E-01
C15-17-2 Locaiton A 10um	500	8.4356E-15		8.4E-12	2.7E-02
Average	500	4.57925E-14		4.6E-11	1.4E-01

Appendix C: All Calculations for Total Deformation

Sample and A & Q Values	Time in years	Velocity (cm/year)		Total Deformation (cm)	Total Deformation (Meters)	Total Deformation (Kilometers)
-A-Q						
C15-11-1	30000000	2.79		83686646	836866.46	836.87
C16-18-1	30000000	13.26		397714197	3977141.97	3977.14
C15-17-2 Location B 5um	30000000	14.96		448854355	4488543.55	4488.54
C15-17-2 Location B 10um	30000000	2.37		71043775	710437.75	710.44
C15-17-2 Location A 5um	30000000	5.78		173351890	1733518.90	1733.52
C15-17-2 Locaiton A 10um	30000000	1.24		37206735	372067.35	372.07
Average	30000000	6.73		201976266	2019762.66	2019.76
-A+Q						
C15-11-1	30000000	0.01		392766	3927.66	3.93
C16-18-1	30000000	0.06		1866588	18665.88	18.67
C15-17-2 Location B 5um	30000000	0.07		2106603	21066.03	21.07
C15-17-2 Location B 10um	30000000	0.01		333429	3334.29	3.33
C15-17-2 Location A 5um	30000000	0.03		813590	8135.90	8.14
C15-17-2 Locaiton A 10um	30000000	0.01		174622	1746.22	1.75
Average	30000000	0.03		947933	9479.33	9.48
Middle A Middle Q						
C15-11-1	30000000	0.65		19595595	195955.95	195.96
C16-18-1	30000000	1.04		31283096	312830.96	312.83
C15-17-2 Location B 5um	30000000	1.18		35305639	353056.39	353.06
C15-17-2 Location B 10um	30000000	0.19		5588106	55881.06	55.88
C15-17-2 Location A 5um	30000000	0.45		13635379	136353.79	136.35
C15-17-2 Locaiton A 10um	30000000	0.10		2926579	29265.79	29.27
Average	30000000	0.60		18055732	180557.32	180.56
+A-Q						
C15-11-1	30000000	12.75		382521775	3825217.75	3825.22
C16-18-1	30000000	60.60		1817904623	18179046.23	18179.05
C15-17-2 Location B 5um	30000000	68.39		2051660244	20516602.44	20516.60
C15-17-2 Location B 10um	30000000	10.82		324732705	3247327.05	3247.33
C15-17-2 Location A 5um	30000000	26.41		792371014	7923710.14	7923.71
C15-17-2 Locaiton A 10um	30000000	5.67		170067593	1700675.93	1700.68
Average	30000000	30.77		923209659	9232096.59	9232.10
+A+Q						
C15-11-1	30000000	0.06		1795285	17952.85	17.95
C16-18-1	30000000	0.28		8531951	85319.51	85.32
C15-17-2 Location B 5um	30000000	0.32		9629034	96290.34	96.29
C15-17-2 Location B 10um	30000000	0.05		1524064	15240.64	15.24
C15-17-2 Location A 5um	30000000	0.12		3718826	37188.26	37.19
C15-17-2 Locaiton A 10um	30000000	0.03		798176	7981.76	7.98
Average	30000000	0.14		4332889	43328.89	43.33

Appendix D: Sample Coordinates

Sample	Latitude	Longitude
C15-11-1	44°15'55.47"N	69°30'48.75"W
C16-18-1	44°20'34.97"N	69°24'48.02"W
C15-17-2	44°15'28.19"N	69°31'26.19"W
C15-04-3	44°16'15.20"N	69°30'14.22"W